

Multiple ash layers in late Quaternary sediments from the Central Indian Basin.

Mascarenhas–Pereira M.B.L.^{1*}, Nath B.N.¹, Iyer, S.D.¹,
Borole, D.V.¹, Parthiban, G.¹, Jijin, R.², and Khedekar, V.¹

¹CSIR National Institute of Oceanography, Dona Paula, Goa, 403 004, India.

²Fugro Survey (India) Pvt. Ltd. Mumbai, 400 706

***Corresponding Author:**

E-mail address: mariab@nio.org (M.B.L. Mascarenhas–Pereira)

Highlights

- Unraveled volcanic history of the CIB since the late Pleistocene.
- Identified four shard-rich horizons (70–75, ~85, 107–109 and 142–146 ka) and a cryptotephra (~34 ka) horizon at different depths from 3 sediment cores.
- Four volcanic horizons were hitherto unknown and do not correspond to any known volcanic eruption in the Indian Ocean.
- Multiple horizons of volcanoclastic materials at water depths >5,000 m indicate that submarine phreatomagmatic eruptions are much more common than previously suspected in intraplate areas.

Abstract

We have investigated three sediment cores collected from water depths >5,000 meters along the transect 76°30'E in close proximity to a fracture zone in the Central Indian Basin (CIB). The cores yielded five volcanic horizons of which four have visual and dispersed shards. Rhyolitic glass shards of bubble wall, platy, angular and blocky types were retrieved from various stratigraphic horizons in the cores. The abundance of glass shards, composition of bulk sediments, and ²³⁰Th_{excess} ages of the host sediments were used to distinguish the volcanic horizons. Of the four volcanic horizons, three are now newly reported and correspond to ages of ~ 85, 107–109 and 142–146 ka while the fourth horizon is of 70-75 ka. By using trace element ratios and Cr and Nb-based normative calculations, cryptotephra has been identified for the first time from the CIB sediment. The cryptotephra forms the fifth ash horizon and is of ~34 ka.

A comparison with the published data on volcanic tephra in and around the Indian Ocean indicate the shard rich horizon (SRH) of 70–75 ka to resemble the Younger Toba Tuffs (YTT), while the other volcanic horizons that were deposited during different time periods do not correlate with any known marine or terrestrial records. These tephra layers have produced a tephrostratigraphic framework across the tectonically and volcanically complex regions of the CIB. Due to the lack of terrestrial equivalents of these tephra, it is hypothesized that the newly found volcanic horizons may have been derived from submarine volcanic eruptions. Multiple layers of submarine volcanoclastic deposits found at water depths as great as 5300 m reaffirm the growing belief that submarine phreatomagmatic eruptions are much more common in the intraplate region of the Indian Ocean than previously reported.

1. Introduction

The occurrence of volcanic ash in marine sediments has long been recognized to be an important component of the global sedimentary system (Scudder et al., 2009). Submarine tephra studies have become increasingly important because distal tephra deposits are often the only indicators for reconstructing the petrogenetic evolution of volcanic terrains that have been eroded or buried under younger sediments (Fisher and Schmincke, 1984; Straub, 1997). Furthermore, the tephra deposits provide a link to past volcanism, climate, volcanic arc evolution, biological productivity and other processes (e.g. Straub and Layne, 2003; Ziegler et al., 2007).

Visible tephra layers are found in a number of areas (e.g., Vityaz Fracture zone on the Indian Ocean ridge, Iceland, Kamchatka, New Zealand, Central Indian Basin etc), and their dispersal could depend on the carrying strength of the transporting media. However, cryptotephra horizons (Lim et al., 2008; Pollard et al., 2006) can occur in distal areas from volcanic sources (e.g. Scudder et al., 2009).

Volcanogenic material such as pumice and glass shards found in the Central Indian Basin (CIB) sediments has been mainly attributed to the distal fallout from Toba, the Indonesian volcanic arc (IVA) or Krakatau volcano (Iyer and Karisiddaiah, 1988; Martin–Barajas and Lallier–Verges, 1993; Mudholkar and Fujii, 1995; Mukherjee and Iyer, 1999; Pattan et al., 1999, 2010). However the origin of silicic material and volcanogenic-hydrothermal material (vhm) was also ascribed to intraplate volcanism in the CIB (Gupta, 1988; Iyer and Sudhakar., 1993; Iyer et al., 1997, 1999, 2007; Sukumaran et al., 1999; Mascarenhas–Pereira et al., 2006, 2010; Kalangutkar et al., 2011). Mascarenhas–Pereira et al. (2006) reported the occurrence of volcanic ash in a sediment core (AAS 61/BC-8) (Table 1) sampled from the flanks of a seamount lying close to a fracture zone that has been identified by Kamesh Raju et al. (1993) and Dyment (1993) as a trace of the Indian Ocean Triple Junction. Although the chemistry of the glass shards studied by Mascarenhas–Pereira et al. (2006) was similar to those originated from Toba, the age (>180 ka) of the shard-bearing sediments was different from the major Quaternary Toba eruptions namely Young, Middle and Old Toba Tuff (YTT, MTT and OTT) and other rhyolitic eruptions in the Indian Ocean. This fact suggests that the CIB sediments could host tephra derived from different sources during other time periods as well.

Here we report the occurrence of four previously undocumented volcanic horizons of late Pleistocene Epoch in three $^{230}\text{Th}_{\text{excess}}$ dated sediment cores collected along a fracture zone (76°30'E) from north to south in the CIB. In addition, for the first time for the Indian Ocean, cryptotephra were identified from geochemical data. Unlike the earlier workers we do not use the ambiguous term 'layer' to describe the occurrence of volcanic shards at various core depths. This is because 'layer' *sensu stricto* has a different connotation and refers to visually distinguishable band or stratum of shards in a sediment core. Since this is not the case in the present study or of those in the earlier reports therefore, we would use the term 'shard-rich horizons' (SRH) for peaks of dispersed ash (mixed in the bulk sediments) identified from tephra counts using a microscope and were also confirmed by chemical normative calculations of bulk sediment data (following Scudder et al., 2009; 2016). We use the term cryptotephra (Lim et al., 2008) for ash layers that were solely identified

using chemical data. The term volcanic horizon has been used collectively for SRH and cryptotephra..

2. Material and methods

2.1. Sample details

The sediments used in this study were recovered using a box corer (Kastengriefer type) of dimensions 50 x 50 x 50 cm during the 61st cruise of R.V.A.A. Sidorenko in the year 2003. Three cores (BC 14, 20 and 25) collected from water depths ranging from 5,000 to 5,300 m in a north–south transect along 75°30'E (Fig. 1) were used for this study. The cores were split at 2 cm interval. The location, water depth, length and a brief description of the cores are provided in Table 1.

2.2. Sedimentological and geochemical methods

Bulk sediments from each of the cores (AAS 61: BC 14, BC 20 and BC 25) were made salt–free by repeated washing with distilled water followed by stirring, in order to disaggregate sediment lumps, if any. The salt freed sediment samples were wet sieved through 63 and 45 μm sieves using distilled water and dried at 60°C. The sediment fractions (<45 μm) were decalcified using acetic acid, centrifuged and treated with H_2O_2 to remove the carbonate and organic matter. The residue was treated with Na_2CO_3 to dissolve biogenic silica. The treated sample residue representing the lithogenic fraction was disaggregated in an ultrasonic bath for 1 min. Grain-size analysis was carried out using an MALVERN Laser Particle Analyzer (LPSA) (MASTERSIZER 2000) fitted with a hydro 2000 MU wet sampling accessory.

The sediment fractions retained on the 63 μm (sand–sized) and 45 μm (coarse silt) sieves were used for microscopy studies. A representative fraction of both the size fractions was obtained using the coning and quartering method. Approximately 0.01g of the size fraction was used to represent a particular sample and studied under a high resolution stereoscopic binocular microscope for the identification, quantification and the general description of the coarse fractions. Glass shard abundance was determined by visually counting them under the microscope and subsequently calculated on per gram basis.

Clean glass shards with no visible alteration features were handpicked from both (45 and 63 μm) size fractions and mounted on brass stubs. Scanning Electron Microscopy (SEM of JEOL JSM-5800LV type) study was performed to examine the shard morphology. The operating conditions were 20 kV accelerating voltage, 55 na probe current and 3–5 μm beam diameter. Major oxides were analyzed using an energy dispersive spectrometer (EDS) attached (OXFORD Link–ISIS EDS) to the SEM. The major elemental data of the shards presented here are for the > 63 μm size fraction. Analytical accuracy derived from repeated analysis of an orthoclase mineral standard is generally better than 7% for K_2O and better than 2% for Al_2O_3 and SiO_2 .

For geochemical studies, bulk sediment samples from the three cores (BC 14, 20 and 25) and the geochemical standards were decomposed using 10 ml of acid mixture containing 6 parts of HF, 3

parts of HNO₃ and 1 part of HClO₄ in Teflon beakers. The solutions were then evaporated to dryness in a fume hood. Addition of acid mixture was repeated to ensure a complete dissolution of the samples. 1 ml of 1 ppm Rh solution and 4 ml of 1:1 suprapure HNO₃ were added to the digested solution and made up to 100 ml. The solutions were used for major element analysis by Inductively Coupled Plasma Optical Emission Spectrometry (ICP–OES), and trace elements by Inductively Coupled Plasma Mass Spectrometry (ICP–MS). Geochemical standards (USGS Marine Mud standard (MAG–1) and Cody Shale (SCo–1)) were used to determine the analytical accuracy. Accuracy of our analytical results is generally better than 10% for Sc, 14% for Cr, 4% for Nb and 2% for Al.

For radiometric dating, about 2–3 g of sediment from each section of the three cores was dissolved using various acids (HF–HClO₄–HNO₃–HCl) in sequence, in the presence of ²⁰⁸Po and ²³²U/²²⁸Th spike. Uranium–Thorium radiochemical separation and purification were carried out following the standard procedures of Krishnaswami and Sarin (1976). The alpha activity of the electroplated sample was assayed using an ion implanted detector coupled to an OCTETE plus Alpha spectrometer (E G & G ORTEC). The values for ²³⁰Th_{excess} were calculated by subtracting the ²³⁴U activity from the total ²³⁰Th activities.

3. Results

3.1. Sedimentological, morphological description and abundance of volcanic glass

The particle-size data (LPSA) (Fig. 2) reveal a bimodal distribution of sizes in all the studied core sections. Higher volume percentage is seen in two size ranges, first between 20 and 50 μm which is coarse and the second between 2 and 5 μm which is fine.

Visual observations of >45 and >63 μm size fractions of the sediment sections revealed abundant glass shards. The abundance of glass shards (no of shards g⁻¹) in the studied cores is shown in Fig. 3. The visual counts data show an abundance of glass shards at two horizons in cores BC 14 at 18–20 cm and 22–24 cm; three horizons in BC 20 at 16–18, 24–26 and 32–34 cm, three horizons in BC 25 at 16–18, 24–26 and 32–34 cm (Table 2, Fig. 3) and below 8 cm bsf in the core BC 8 (Mascarenhas-Pereira et al., 2006).

The microscopy investigations show that the glass shards are fresh, shining and colorless that indicate of a silicic composition (Horn et al., 1969). The shards are of different sizes (45–250 μm) and shapes and with no signs of alteration. There are four different types of shards (Fig. 4) in all the cores: 1) blocky with a few vesicles (Fig. 4a), 2) bubble walled or Y-shaped with smooth and slightly curved surfaces (Fig. 4b), 3) angular, moderately vesicular shards with tubular vesicles that extend along the length of the shard (Fig. 4c), and 4) platy (Fig. 4d). These are similar to those reported by Mascarenhas-Pereira et al. (2006). The shards range in morphology from highly vesicular to poorly vesiculated and blocky/massive. The coarse fraction of the sediments also contains micronodules, bioclasts and lithic fragments (e.g. quartz, plagioclase, altered basalt pieces etc).

3.2. Radiometric dating

The sediments were radiochemically dated using $^{230}\text{Th}_{\text{excess}}$ method (excess portion of the ^{230}Th that is not supported by the decay of ^{234}U in the sediments; half life = 75200 y). Radiometric ages were obtained from the down-core distribution of $^{230}\text{Th}_{\text{excess}}$ activity (Borole, 1993), assuming constant sediment accumulation rate at the core sites. The measured $^{230}\text{Th}_{\text{excess}}$ activity is a function of depth for BC 14, 20 and 25. The decay curve of $^{230}\text{Th}_{\text{excess}}$ for sediment section between the surface (0 cm) and the bottom of the cores (26 cm for BC 14 and 34 cm for BC 20 and 25) is linear with depth and involved a single slope averaged over the entire core depth (Fig. 5). The estimated sedimentation rates are 0.27 cm ka^{-1} for BC 14 and 0.23 cm ka^{-1} for both the cores BC 20 and BC 25. The overall maximum uncertainty associated with constant sedimentation rate using Criss Cross method is estimated to be $\sim 14\%$. Given the uncertainty, the agreement between the ages of volcanic horizons appears to be reasonable. The average rate of sedimentation (0.25 cm ka^{-1}) for the three cores testifies that any influx of matter to the area was constant and did not disturb the natural distribution and therefore bioturbation can be ruled out.

3.3. Glass shard composition

Major element data of all the four morphological types of shards are presented in Table 3. The salient features of the volcanic horizons from the three cores are synthesized in Table 4. No significant change in major oxide composition was seen as a function of glass morphology. In the present study, major oxide (wt %) Si, K, Na data of the glass shards from BC 14, 20 and 25 SRH are plotted in the TAS diagram (Fig. 6). The glass shards are rhyolitic with a range of SiO_2 between ~ 77 and $79 \text{ wt}\%$, and display a range of total alkalis ($\text{Na}_2\text{O} + \text{K}_2\text{O}$) from 7.63 to $9.45 \text{ wt}\%$ (Fig. 6, 7). The elemental compositions of the tephra from the SRH are compositionally similar in all the three cores (Fig. 7), irrespective of the core depth with a marginal variation in elemental composition (Table 2). A comparison of our data with the earlier reports (Mascarenhas-Pereira et al., 2006 and references therein) shows a close correspondence and further attest the rhyolitic nature of the shards.

3.4. Geochemistry of bulk sediments

The bulk sediments from the three cores were analyzed for 7 major elements by ICP-OES and 40 trace elements by ICP-MS, however only certain elements such as Al, Cr, Nb and Sc are being used (Table 2) which have relevance to the present study. These elements were used in the normative calculation to determine the presence of discrete ash component in the sediments. Sc is generally high (upto 19 ppm) in the surface sediments and decreases with depth and the lowest concentration (12 ppm) is found in BC 20 and BC 25 at 32-34 cm bsf. Cr also displays a trend similar to Sc in BC 20 and 25; however with no clear trend in BC 14.

4. Discussion

Prior to delving into the discussion it would be pertinent to clarify certain aspects that may have a bearing on the distribution, characteristics, composition, source and age of the volcanic horizons. The premises that we have considered are as follows.

1) *No bioturbation effects*: We rule out bioturbation process to have influenced the occurrence of the volcanic horizons at different depth levels in all the three cores. This is because, and as also stated earlier, the plot of $^{230}\text{Th}_{\text{excess}}$ (dpm g^{-1}) vs. core depth (Fig. 5) shows a single slope which would not be the case if bioturbation had caused mixing of the sediments. Further, $^{210}\text{Pb}_{\text{excess}}$ (half life = 22.5yr) was present only in the top 2 cm sections (Borole, 1993) of the CIB sediments indicating that the benthic mixing is confined to the top 2cm.

2) *No alteration of glass*: Microscopy observations depict the shards to be fresh and with insignificant alteration and hydration rinds (Fig. 4). Moreover, the shards from different depth levels have consistent alkali values on par with those reported by previous workers and corroborate to the negligible alteration effects undergone by the SRH.

3) *Absence of altered material*: The SRH are characterized by the lack/very low abundance of altered material such as palagonite or iron-rich fragments. This again is evident of the absence of alteration of the core sediments.

Therefore, the occurrence of volcanic horizons in the three cores may represent that the stratigraphy of the cores is ‘undisturbed’ and the glass composition as chemically unaltered.

4.1. Bimodal particle size distribution

The first peak in the size data (Fig. 2) (2 to 5 μm size) can be considered to be the clay component in the sample while the coarser/second peak (20 to 50 μm) represents silt size particles. Clay minerals in the CIB are contributed from three sources, viz., (i) through turbidity currents via the Bay of Bengal derived from Ganges–Brahmaputra rivers (Rao and Nath, 1988; Nath, 2001), (ii) aeolian transport from distal areas such as South Africa and Australia (Fagel, 2007; Nath et al., 2013 and references therein), and (iii) the alteration of basinal volcanic rocks (Rao and Nath, 1988; Iyer, 1999; Nath, 2001). On the other hand, the coarse peak of medium coarse–silt range would either represent biogenic silica or volcanic shards, both of which are abundant in the basin. Since, the samples were treated with Na_2CO_3 , which has dissolved the opaline silica; this size fraction is composed mainly of volcanic shards. Microscopy observation has also shown this fraction to be dominated by glass shards.

4.2. Glass shard morphology

Glass shard morphologies in all the three cores indicate two shard populations at different depths. The shallow (18-20 cm in BC 14; 16-18 cm in BC 20 and BC 25) SRH with an age of 70-75 ka is dominated by bubble wall shards, while the deeper (22-24 cm in BC 14; 24-26 cm in BC 20 and BC 25) horizons are dominated by massive, blocky types (Fig. 4a) with a minor component of bubble wall shards (Fig. 4b).

Platy shards (Fig. 4d), formed from the glass walls separating large flattened vesicles and angular shards (Fig. 4a, c), which are moderately vesicular with tubular vesicles that extend the length of the shard are also present in the cores. The shards range from highly vesicular to poorly vesiculated and blocky/massive typically indicating a submarine source (Wohletz, 1983; Fisher and Schmincke,

1984). The vesicles coalesce to give rise to a tubular morphology (Fig. 4a). The glass shards have conchoidal to (irregular) angular fractures that likely record a phreatomagmatic activity of rapid quenching and fragmentation during interaction between magma and water.

4.3. Composition of shards

Based on chemistry of the shards and age of the sediments, an attempt is made to identify the possible source(s) of the shards to the study area with those that erupted in and around the CIB. There are number of possible sources that could have contributed to the volcanogenic material to the area such as the Reunion hotspot, the Kerguelen plume, Broken ridge, Indian Ocean Ridge volcanic, Afro-Arabian flood volcanism, the Taupo volcanic center (New Zealand) and distal fallout from the Youngest Toba Tuffs of Sumatra (Mascarenhas-Pereira et al., 2006 and references therein). Most of the volcanic products from the probable sources are dominantly of effusive basaltic volcanism type (Reunion, Kerguelen hotspots tract, Indian Ocean ridge system and Broken ridge) and therefore cannot be a potential source for our shards. Though the Afro-Arabian flood volcanism and the Taupo volcanic center have a similar range of silica as in our shards, the depositional ages (~30 Ma and 26.5 ka, respectively) do not permit a direct correlation (Mascarenhas-Pereira et al., 2006).

To chemically distinguish the different ash layers a plot of total alkalis against silica (TAS diagram) was used to facilitate distinction between alkaline and sub-alkaline suite. All the data points from the individual volcanic horizons from the three cores plot within the rhyolitic field (Fig. 6a). The high silica field can be subdivided into low, medium and high K groups. It is apparent that all the tephra from the individual SRH from BC 14, BC 20 and BC 25 plots distinctly in the high K_2O series (Fig. 6b). Published data of glass shards from different locations from the Indian Ocean for Toba units (OTT: Dehn et al., 1991; Glass and Koeberl, 2006; Pattan et al., 2010; Lee et al., 2004; YTT: Shane et al., 1995, Pattan et al., 1999) are plotted along with our data (Fig 6). Though the rhyolitic volcanics of the present study, YTT, OTT are of different ages (present study: ~70-180 ka; YTT: 75 ka and OTT: 840 ka) do not show significant variation in their chemistry (Fig. 6) and fall in the high K_2O series. Given the uncertainty of SiO_2 data of our analysis (2 %), our SHR falls in the general spread of previous reports of YTT data. The above observation indicates that irrespective of the depth of occurrence of the shards and their ages (to be discussed later), there are insignificant compositional differences. This also suggests that not all rhyolitic ashes found in the Indian Ocean can be from a single source. Moreover, while the dominant type shard morphology of Toba volcanics is bubble wall type (Rose and Chesner, 1987), the major morphological type in deeper sediment layers of the cores studied is massive/blocky suggesting a different source possible a local source. This point to the fact that rhyolitic/silicic eruptions perhaps prevailed at localized sites in the CIB (cf. Iyer and Sudhakar, 1993; Kalangutkar et al., 2011).

4.4. Age of the volcanic horizons

In Figure 5, the ages of the sediment sections are plotted as a function of depth to estimate the depositional ages of the ash layers. The base of the cores correspond to ~92 ka for the sediments at 26 cm for BC 14, 146 ka for the sediments at 34 cm for BC 20 and ~142 ka at the base of 34 cm for

BC 25. Low sedimentation rates found here (Fig. 5) were also been reported for various locations in the CIB, e.g., 0.032 cm ka^{-1} on the flanks of a seamount by Mascarenhas–Pereira et al. (2006), and 0.062 cm ka^{-1} on top of a seamount by Nath et al. (2013). Pattan et al. (2010) have reported two rates of sedimentation for post-YTT (0.17 to 0.45 cm ka^{-1}) and pre-YTT (0.07 to 0.163 cm ka^{-1}) but in the absence of a change in $^{230}\text{Th}_{\text{excess}}$ profiles (above and below glass shard horizons), it is difficult to concur with their observation. Although core BC 14 records two independent SRH of 70.6 and 85.5 ka age based on abundance of shards (18-20 and 22-24 cm, respectively), they are fairly close in age given the uncertainty of 13.88% associated with constant sedimentation rate based age depth model. However, the two SRH (18-20 and 22-24 cm) are separated by a low abundance shard layer (20-22 cm) suggesting that they may be two SRH as previously proposed.

Sediment of cores BC 25 and 20 record a longer age span (142 and 146 ka, respectively) as compared to BC 14 which extends to ~ 92 ka. The SRH occurring at shallow depth (18-20 in BC 14; 16-18 cm in BC 20 and 25) in the three cores display a maximum age of ~ 74 ka, while the deeper (22-24 cm in BC 14; 24-26 cm in BC 20 and 25; > 8 cm bsf in BC 8) SRH exhibit a maximum age of > 180 ka (Mascarenhas-Pereira et al., 2006). An important observation here is that the abundance of shards of a particular age is consistently found at approximately at the same stratigraphic positions in the three cores. For example, the 75 ka YTT event occurs at 18-20 cm in BC 14 and 16-18 cm in BC 20 and BC 25, while the 107-109 ka volcanic event is reflected at 24-26 cm in the cores BC 20 and BC 25 (Table 3).

4.5. Determining of dispersed ash and cryptotephra in sediments

The SRH were identified from visual observations under a microscope. However, dispersed ash is invisible to the naked eye and thus difficult to identify on account of the very fine grain size of the shards and their alteration to authigenic clays (Scudder et al., 2009; 2016). Thus, we inferred the occurrence of dispersed ash from the chemical signatures present in the cores. Cryptotephra, on the other hand are generally dominated by glass shards finer than $80 \mu\text{m}$ in diameter (Basile et al., 2001; Turney et al., 2004) but in low concentration thus making estimation by visual techniques impossible. They may be distributed hundreds of kilometers from the source (Pollard et al., 2006) which can be the result of small to moderate eruptions, long distance from the source volcano, or due to bioturbation (Lowe and Turney, 1997). Many methods such as Cr and Nb based normative calculations (Peters et al., 2000; Scudder et al., 2009; 2016), and trace elemental ratios (Lim et al., 2008) are used to estimate and quantify the dispersed ash and cryptotephra content respectively in the sediments.

Considering the down-core geochemistry of the bulk sediments generated for this study, we have used the single element normative calculation based on Urbat and Pletsch (2003) and Scudder et al. (2009). Urbat and Pletsch (2003) used normative calculations on the basis of Al and Cr contents to discriminate between the major groups of components (terrigenous, volcanogenic, biogenic, and diagenetic). Accordingly, we have normalized the Al concentration in each sample to average shale to estimate the total amount of “terrigenous component and ash” (Plank et al., 2000) on the premise

that the Al concentrations in the ash and terrigenous material are approximately equal to average shale (Al = 8.84%) (Chester, 1990). Concentrations of Nb and Cr were then used to calculate the amount of terrigenous material, with dispersed volcanic ash being subsequently determined by its difference. Two key assumptions were made for both the methods. In case of Cr based normative calculations, we assumed that all Cr is in the terrigenous components and that the volcanic components contributes little Cr. Secondly, we assumed that the Al and Cr concentrations in the respective components correspond to the concentrations of these elements in average shale. The latter assumption seems warranted because the discrete volcanic horizons contain only very low Cr content (17–38 ppm) (Lim et al., 2008) compared to its concentration in average shale (110 ppm) (Taylor and McLennan, 1985).

In case of Nb based normative calculations, Nb is enriched in average shale (19 ppm; Taylor and McLennan, 1985) and commonly depleted in ashes (0.5–6 ppm; Taylor and Nesbitt, 1998) and rhyolites (~3.09 ppm; Scudder et al., 2009) similar to the concentration found in the sediments of the study area (3.07–7.84 ppm, Table 2). The Nb-based normative calculations suggest that 19–29 wt% of the studied sediments is dispersed ash, compared to 26–31% of dispersed ash estimated using Cr-based normative calculations (Fig. 3), however the overall trend and the stratigraphic position of SHR (Fig. 3) using both these methods are similar and consistent with the visual estimates of ash in the cores. The error in the estimated content (%) of dispersed ash is minimal for Nb and Cr based normative calculations (<1 and 3%, respectively). The offset in the ash content (between Nb and Cr-based methods) especially in the lower half of core BC 20 (Fig. 3) seems to be controlled by the presence of manganese micronodules which were noticed under the microscope in these sections. Their macroscopic counterparts (manganese nodules) are typically known to have low Cr (only element close to crustal values) and high Nb content (e.g. Cronan, 1976). However, both these methods (Cr and Nb based calculations) will not resolve the compositional variation within the total bulk ash inventory, nor can they help identify the source of the volcanic ashes in the sediments (cf. Scudder et al., 2009) but will only help to estimate the volcanic ash content.

Elements such as Cr and Sc are thought to be the most suitable components for provenance determination because they are refractory in nature and relatively immobile during weathering, sedimentation and diagenetic processes (Taylor and McLennan, 1985). These elements are incorporated into the clastic sediments with little fractionation and are expected to reflect the signature of the parent material (Taylor and McLennan, 1985, McLennan, 2001). We have used Cr/Sc as a tool to detect cryptotephra (Lim et al., 2008) and as a means to identify the probable stratigraphic positions of distal/proximal cryptotephra in the CIB pelagic sediments. The low Cr/Sc ratios at the depths coinciding with high abundance of shards indicate the usefulness of this ratio. A comparison of the Cr/Sc ratio and the abundance of glass shards (no of shards g⁻¹) in the bulk sediments (Fig. 3, Table 2) show a similar pattern between the two in terms of timing and overall trend. There are three notable features of this comparison.

- 1) First, the “dips” in the ratio coincide with the high abundance of shards in the cores.

2) The ~74 ka and the ~ 85, 107–109 and 142–146 ka volcanic events are clearly marked by an increased abundance of glass shards as well as the low Cr/Sc ratio (Fig. 3).

3) We deciphered a cryptotephra within the core BC 14 (Fig. 3) that corresponds to ~34 ka and this volcanic event is much younger than the (70–75 ka) YTT. A comparison of the record of all the sites and the accumulation rate of the shards also show a similar pattern in terms of timing and the general trend. The abundance of shards in the >63 µm coarse fraction, accumulation rates as well as the Cr/Sc ratio, which indicates the cryptotephra horizon at 8–10 cm bsf in core BC 14 (age ~34 ka), synchronize well and indicate an increase in accumulation rates around ~70–75 ka and with the other peaks at ~ 85, 107–109 and 142–146 ka.

4.6. Possible origin of volcanic horizons

There is a growing evidence of explosive pyroclastic eruptions occurring in the deep sea. The physical model developed over the past several years for submarine pyroclastic eruptions (Clague, 2009; Clague et al., 2003a, b; Davis and Clague, 2003; Head and Wilson, 2003; Helo et al., 2008, 2011) suggests that pyroclastic fragments are produced by CO₂-driven explosive events accompanying effusive activity (Helo et al., 2013). In the course of an explosive submarine eruption, the particles are entrained into a rising eruption plume and widely dispersed (Barreyre et al., 2011) into the surrounding areas. Head and Wilson (2003) suggested that the most efficient transfer of magmatic gas into the seawater above the vents occurs in the strombolian eruption, where large gas bubbles are segregated from the magma and erupted directly into the seawater. In a contrasting model, bubble wall shards (Limu ó Pele) are thought to have a pure hydrovolcanic origin, originating from the interaction of sheet lava and seawater, i.e., bursting of seawater steam-bubbles rising through a sheet lava flow (e.g., Maicher and White, 2001; Schipper and White, 2010).

The shapes of individual fragmented clasts are usually related to mode of interaction of the clasts with water (Wohletz, 1983). The blocky shards with a few vesicles, showing spherical to oval shape are typically formed by hydroclastic processes. The bubble walled or Y-shaped shards (Fig. 4b) with smooth and slightly curved surfaces, represent the remnants of three bubble junctions, or double concave plates that form the wall between adjoining bubbles (Fisher and Schmincke, 1984) are typical of explosive volcanism and were probably formed sub-aerially. The co-occurrence of bubble wall shards (Fig. 4b) and massive/blocky shards (Fig. 4a) in the different SRH (~ 85, 107–109 and 142–146 ka) indicates that another mechanism may be responsible for their formation rather than aerial explosive volcanism. Recent studies have shown that a range of pyroclastic deposits of lapilli to ash-sized fragments from explosive submarine activity occur throughout the depth range of observations in the deep-sea (Clague et al., 2009). Such deposits probably form due to the presence of a summit magma reservoir, which favor the build-up of magmatic foams and episodic dike emplacement (Head and Wilson, 2003). This is consistent with the various morphological types of glass shards (Fig. 4) encountered in the study area.

Therefore, the occurrence of bubble wall shards at depths below the critical pressure of water (~3200 m water depth, Mühe et al., 1997) and stratigraphic location of the shards of the same ages in cores

separated by a distance of ~300 km support a pyroclastic origin for the glass shards. Similar glass chemistries and morphologies were also found in the sediments from the southern area (BC 8, 16°S) (Mascarenhas-Pereira et al., 2006) corresponding to an age of ~180 ka which did not correspond to any known eruptions in the area. The source for these shards was attributed to intraplate volcanism, triggered by activation of tectonic activity in the fracture trace of the Indian Ocean Triple Junction during the Late Pleistocene.

Abrupt changes in abundance of volcanoclastic shards at stratigraphic boundaries indicate their relation with multiple episodes of explosive eruptions rather than distance from a source, which would result in a more gradual variation at the depositional sites. Overall, there is no clear gradient in volcanoclastic abundance for the older (>75 ka) three horizons except for the SRH at 75 ka which records a gradual increase in abundance of shards from 18-20 cm (BC 14) and 16-18 cm (BC 20 and 25) to the surface as would be expected with increasing proximity to an explosive source. There is also an increase in abundance of shards (Table 3) at a given SRH (107-109 ka and 141-146 ka), from south to north with BC 25 having a maximum abundance compared to BC 20 and BC 14 which lies at 11°, 12° and 14°S respectively. The southernmost core in the study at 16°S records a volcanic event >180 ka (Mascarenhas-Pereira et al., 2006), while the younger volcanic events recorded in the northern sites (BC 14, 20 and 25 at 14°, 12° and 11°S respectively) are absent. Therefore, if a single explosive source were to be invoked, it would have to be probably at/near (~ 11°S) or two sources, one for the sites north of 14° and the second one closer to 16°S.

There is a strong evidence for the submarine origin of tephra older than 74 ka as there are no known subaerial counterparts of comparable ages within the potential source region. The only possible large subaerial volcanic events that occurred near and within the time frame of the present study is Toba eruption which led to widespread ash dispersion in the Indian Ocean. The Toba eruptions were identified as OTT (Older Toba Tuff) at $840,000 \pm 30,000$, MTT (Middle Toba Tuff) at $500,000 \pm 5,000$ and YTT (Younger Toba Tuff) at $73,000 \pm 4,000$ yrs BP (Diehl et al., 1987; Chesner et al., 1991). The age of the youngest shard layer (70-75 ka) in our study area is similar to the YTT as reported by Chesner et al. (1991) and Pattan et al. (1999). The ages of the older three horizons in the CIB (~ 85, 107-109 and 142-146 ka) do not relate to any of the other two reported Toba events. One possibility of tephra deposition in the study area could be through the redistribution of older material (pre-YTT) from the north by turbidity currents. The Ganges-Brahmaputra/Bengal fan sediments have been reported to reach the CIB through turbidity currents (Pimm, 1974). Sedimentological, clay mineralogical and geochemical studies of the CIB sediments (Pimm 1974; Rao and Nath., 1988; Nath et al., 1989; 1992) indicate that the Ganges-Brahmaputra (G-B) riverine influx is limited to the northern part of the CIB upto 8°S (see the review of Nath 2001). The active turbiditic channels bringing sediments from G-B Rivers are confined closer to the equator in the northern part of the basin and the fan limits do not cross about 5°S (e.g., Emmel and Curray, 1984). The seafloor morphology distinctly changes from a smooth sedimented abyssal plain to structurally deformed area at about 6-7°S in the CIB (Krishna et al., 1998). Further there is a profusion of seamounts south of 12°S (Das et al., 2007), possibly limiting the extent of turbiditic sedimentation in the CIB. The

southern boundary of the Bengal fan limits may be either due to equatorial divergence which acts as a barrier against the northern terrigenous input beyond this latitude or this may be an ultimate stage of dilution (e.g., Debrabant et al., 1993). Moreover the study area has a gradual sedimentation rates with depth with no recorded pulse of increased sedimentation in the sediment cores (Fig. 5) which argues against the pulses of turbiditic events to the area. Another notable observation is that the older volcanic events (107-109 and 142-146 ka, respectively) are recorded in the cores BC 20 and 25 at the same depth horizon (22-24 and 32-34 cm respectively) despite the cores being separated by a degree latitude (~110 km). Thus, we discount the possibility of products derived from pre-YTT events to have contributed the shards in the study area through turbiditic currents.

4.7. Comparison with previous studies on CIB shards

The chemistry of the volcanic shards usually enables correlation of distal volcanic ash units with a known eruption. Analyses of glass composition of tephra throughout the Indian subcontinent provide an evidence for a direct correlation with YTT (Westgate et al., 1998). Many tephra beds, pumice clasts and dispersed glass shards have been found in the Pliocene and Quaternary deep sea sediments of the CIB (Iyer and Sudhakar, 1993; Martin-Barajas and Lallier-Verges, 1993; Pattan et al., 1999, 2010). They have been assigned to various sources like distal fallout from the Youngest Toba eruptions of Sumatra (Martin-Barajas and Lallier-Verges, 1993; Pattan et al., 1999; see Nath, 2001 for a review), Krakatau volcano (Mudholkar and Fujii, 1995) and intra-basinal volcanism (Gupta, 1988; Iyer et al., 1997; Sukumaran et al., 1999; Mascarenhas-Pereira et al., 2006; Kalangutkar et al., 2011). Although Martin-Barajas and Lallier-Verges (1993) suggest an Indonesian arc source for the CIB tephra, but the low alkalis they report do not suggest a direct Indonesian source.

Several magmatic systems over time systematically produce distally dispersed tephtras with very similar (often indistinguishable) major element chemistries such as Katla, Iceland (8500 yrs; Haflidason et al., 2000; Davies et al., 2004), Mount St Helens (275 ka; Busacca et al., 2001) and Campanian province (39-41 ka; Wulf et al., 2004; Smith et al., 2011). Therefore, the glass chemistry normally used to distinguish individual volcanic horizon of different eruption units cannot be solely relied upon to identify chronostratigraphic markers in their distal deposits (Smith et al., 2011). The similarities in major and trace element glass chemistry for the three largest Toba eruptions (OTT, MTT and YTT) which are compositionally similar (Smith et al., 2011) suggest that the tephra horizons in deep sea cores may have been miscorrelated in the past, particularly in sequences which do not have independent chronological control (see Mascarenhas-Pereira et al., 2006; Matthews et al., 2012). Therefore, glass composition may not be a sole viable tool to help identify volcanic horizon that contain distal ash derived from different eruptive phases.

In the present study, the chemistry of the first SRH with an age of ~74 ka correlates well with the previously established age of YTT. This horizon occurs in all the cores and attests to widespread distribution of YTT in the CIB (Dehn et al., 1991; Schulz et al., 1998; Pattan et al., 1999). Several studies of the CIB reported Toba tephra, with the ODP 758 core which is within the 1000 km radius off Sumatra containing deposits of all three (YTT, MTT and OTT) of the large Toba eruptions (Dehn

et al., 1991; Westgate et al., 1998; Lee et al., 2004). This indicates a distal fall-out facies from a large subaerial event like YTT. Therefore the ages of deeper horizons of ash in our cores seem to indicate a source other than Toba to have contributed these SRH in the CIB.

4.8. Possible mechanism of formation

The morphological characters and composition of the shards, location of the cores near the fracture one (Fig. 1) and their age plausibly indicate an in situ / intraplate origin for the shards. In our case we revoke the phreatomagmatic (hydrovolcanic) eruptive mechanism to account for the volcanic horizons in the three sediment cores, as was the case for core BC 8 (Mascarenhas, 2015; Mascarenhas-Pereira et al., 2006) that is located to the south of core BC 14 (Fig. 1). Similar, intraplate volcanic-hydrothermal activity has also been reported from a seamount at 12°S (Iyer et al., 1997). Experimental studies by Wohletz (2003) indicated that hydrovolcanism could occur in water depth > 4,000 m although the products of such an activity are more common in areas of shallow water depths such as seamounts and Mid-ocean ridge (MOR).

Submarine pyroclastic eruptions occur at shallow water depth (< 2000 m water depth) on the Azores Plateau (Fouquet et al., 1998; Eissen et al., 2003), Loihi Seamount and Kilauea Volcano (Clague et al., 2000), however evidence of pyroclastic material at water depths greater than 3,000 m (the critical depth for steam; White et al., 2003) is limited because of the hydrostatic pressure suppresses juvenile gas exsolution so that magmatic disruption and pyroclastic activity are hindered. However, recent studies on the ultraslow-spreading Gakkel Ridge, Arctic Basin, revealed a large (>10 km²) area covered with unconsolidated pyroclastic deposits, including bubble wall fragments (Limu ó Pele), in the axial valley at 4,000 m water depth (Sohn et al., 2008). Helo et al. (2011) measured high CO₂ concentration (> 9000 ppm) dissolved in a Mid Ocean Ridge Basaltic melt. Accumulation of CO₂ in the reservoir is now thought as a potential trigger of explosive eruptions (Pontbriand et al., 2012). These observations demonstrate that large-scale pyroclastic activity is possible along even the deepest portions of the global MOR volcanic system.

The above are examples of Strombolian type (bubble burst) activity that may result in basaltic pyroclasts which may occur at the sea floor if gas exsolution and expansion occur during the slow rise of an erupting dyke, and the rising bubbles coalesce in the upper few hundred meters of the oceanic crust (Head and Wilson 2003). The presence of bubble wall shards in our samples is consistent with some level of subdued explosive activity, but bubble coalescence and fragmentation in the shallow crust can only distribute pyroclasts to distance of ~20–40 m from the source vent (Head and Wilson, 2003). Settling velocity experiments and modeling by Barreyre et al. (2011) found that a buoyant plume of hydrothermal fluid during an eruption (i.e., hydrothermal megaplume) could disperse clasts to at most ~ 400 m from a source vent (assuming nominal current speeds of ~1 cm/s (Stranne et al., 2010) which is inconsistent with the widespread distribution of material over the >300 km² region observed in our study area. However, if fragmentation occurs deeper within the crust and formed due to accumulation of a large volume of volatiles in the upper layer of a crustal magma chamber (Bottinga and Javoy, 1990), then it would create a more violent and explosive

activity spreading pyroclastic material over large areas proportional to the chamber depth (Shon et al., 2008). At the present juncture it is difficult to arrive at a single mechanism that could better account for the occurrence of volcanic shards spread over 300 km² of the study area in the CIB.

5. Conclusion

A detailed investigation of three sediment cores revealed morphological and geochemical evidence for the presence of five volcanic horizons in late Quaternary sediments in the Central Indian Basin and four of these horizons were so far unknown. These volcanic horizons span a time period of the last 150 ka volcanic history of the CIB. Sedimentological studies of the bulk samples show a distinct bimodal size distribution (2–5 and 20–50 µm) in all the sections of the cores, the coarser peak representing volcanic ash which is abundant in the cores.

Of these five horizons, microscopy studies reveal distinct SRH that were identified using visual techniques. These correspond to ~ 85, 107–109 and 142–146 ka age, in addition to the previously documented SRH of ~75 ka (YTT) and >180 ka. Furthermore for the first time dispersed ash was quantified and cryptotephra were identified from the CIB based on normative calculations and trace element ratios. This cryptotephra has an age of ~ 34 ka. The hitherto unknown older events (~ 85, 107–109, 142–146 ka) and the cryptotephra do not correspond to any known volcanic eruption in the Indian Ocean.

The glass shards are rhyolitic and seem to have been derived from either a single source or multiple sources with similar compositions. Ruling out terrestrial volcanic sources, except for the SRH that has YTT shards, the other possibility is of an intraplate volcanism. Fragmentation of the magma deep within the crust formed due to accumulation of a large volume of volatiles would create a more violent and explosive pyroclastic activity spreading material over large areas. Multiple horizons of volcanoclastic materials found at water depths as great as 5,000 m indicate that submarine phreatomagmatic eruptions are perhaps much more common than previously suspected in intraplate areas.

Acknowledgements

We thank the Director, CSIR-NIO for permission to communicate this manuscript. Sediments used in this work were collected under the project “Environmental Impact Assessment of Nodule Mining” funded by the Ministry of Earth Science, New Delhi. We acknowledge the help rendered by Ms Sampada for carrying out the microscopy analysis, Dr M. Desa for generating figure 1, Ms Trupti Naik and Mr Vijayan for radiometric dating, Dr R. Agnihotri for help with estimating the errors, Mr Areef Sardar for SEM and EDS analysis and Ms Nila for the ICP–MS analysis. Dr V.K. Banakar helped during the ICP-OES analysis. We profusely thank an anonymous reviewer and Dr. C. Helo for their invaluable suggestions that vastly changed the presentation and discussion of the data. Prof. L. Wilson (Journal Editor) is acknowledged for encouraging us to revise the manuscript. This is a contribution to the CSIR Network Project GEOSINKS. This is NIO’s contribution No.

References

- Barreyre, T., Soule, S.A., Sohn, R.A., 2011. Dispersal of volcaniclasts during deep-sea eruptions: settling velocities and entrainment in buoyant seawater plumes. *J. Volcanol. Geotherm. Res.*, 205, 84–93.
- Basile, I., Petit, J.R., Touron, S., Grousset, F.E., Barkov, N., 2001. Volcanic layers in Antarctic (Vostok) ice cores: Source identification and atmospheric implications. *J. Geophys. Res.*, 106, 31915–31931.
- Borole, D.V., 1993. Late Pleistocene sedimentation: A case study of the central Indian Ocean Basin. *Deep-Sea Res.*, 40, 761–775.
- Bottinga, Y., Javoy, M., 1990. Mid-ocean ridge basalt degassing: Bubble nucleation. *J. Geophys. Res.*, 95, 5125–5131.
- Busacca, A. J., Marks, H. M., Rossi, R., 2001. Volcanic glass in soils of the Columbia Plateau, Pacific Northwest, USA. *Soil Sci. Soc. Am. J.*, 65, 161–168.
- Chesner, C.A., Rose, W.I., Deino, A., Drake, R., Westgate, J.A., 1991. Eruptive history of the Earth's largest Quaternary caldera Toba, Indonesia clarified. *Geol.* 19, 200–203.
- Chester, R., 1990. *Marine Geochemistry*. London, Boston, Sydney, Wellington: Unwin Hyman, 698 pp
- Clague, D.A., Davis, A.S., Bischoff, J.L., Dixon, H.E., Geyer, R., 2000. Lava bubble-wall fragments formed by submarine hydrovolcanic explosions on Loihi Seamount and Kilauea Volcano. *Bull. Volcanol.*, 61, 437–449.
- Clague, D.A., 2009. Accumulation rates of volcaniclastic deposits on Loihi Seamount, Hawaii. *Bull. Volcanol.*, doi:10.1007/s00445-009-0281-y
- Clague, D.A., Batiza, R., Head, J.W.I., Davis, A.S., 2003a. Pyroclastic and hydroclastic deposits on Loihi Seamount, Hawaii. In: White, J.D.L., Smellie, J.L., Clague, D.A. (Eds.), *Explosive subaqueous volcanism*. *Am. Geophys. Union Geophys. Monogr.* Washington D.C. 140, 73–95.
- Clague, D.A., Davis, A.S., Dixon, J.E., 2003b. Submarine strombolian eruptions on the Gorda Mid-ocean ridge. In: White, J.D.L., Smellie, J.L., Clague, D.A. (Eds.), *Explosive subaqueous volcanism*. *Am. Geophys. Union Geophys. Monogr.* Washington D.C. 140, 111–128.
- Cronan, D.S., 1976. Basal metalliferous sediments from the eastern Pacific. *Geological Society of America Bulletin* 87, 928-934.
- Davies, S.M., Wohlfarth, B., Wastegård, S., Andersson, M., Blockley, S., Possnert, G., 2004. Were there two Borrobol Tephra during the early Late-glacial period: implications for tephrochronology? *Quat. Sci. Rev.*, 23, 581–589.
- Davis, A.S., Clague, D.A., 2003. Hyaloclastite from Miocene seamounts offshore central California: compositions, eruption styles, and depositional processes. In: White, J.D.L., Smellie, J.L., Clague, D.A. (Eds.), *Explosive subaqueous volcanism*. *Am. Geophys. Union Geophys. Monogr.* Washington D.C. 140, 129–142.

- Debrabant, P., Fagel, N., Chamley, H., Bout, V., Caulet, J.P., 1993. Neogene to Quaternary clay mineral fluxes in the Central Indian basin. *Palaeogeography, Palaeoclimatology, Palaeoecology* 103, 117–131.
- Das, P., Iyer, S.D., Kodagali, V.N., 2007. Morphological characteristics and emplacement mechanism of the seamounts in the Central Indian Ocean Basin. *Tectonophysics* 443, 1-18.
- Dehn, J., Farrel, J.W., Schmincke, H.-U., 1991. Neogene tephrochronology from site 758 on Ninety East Ridge: Indonesian arc volcanism of the past 5 Ma. *Proc. ODP, Sci. Results.* 121, 273–295.
- Diehl, J.F., Onstott, T.C., Chesner, C.A., Knight, M.D., 1987. No short reversals of Brunhes age recorded in the Toba Tuffs, north Sumatra, Indonesia. *Geophys. Res. Lett.*, 14, 753–756.
- Dyment, J., 1993. Evolution of the Indian Ocean Triple Junction between 65 and 49 Ma (anomalies 28 to 21). *J. Geophys. Res.*, 98, 13,863-13,878.
- Emmel, F.J., Curray, J.R., 1984. The Bengal submarine fan, Northeastern Indian Ocean. *Geo-Mar. Lett.*, 3, 119-124.
- Eissen, J.-P., Fouquet, Y., Hardy, D., Ondreas, H. 2003. Recent MORB volcanoclastic explosive deposits formed between 500 and 1750 m.b.s.l. on the axis of the Mid-Atlantic Ridge, south of the Azores. pp. 143–166. In: White, J.D.L., Smellie, J.L., Clague, D.A., (Eds.), *Explosive Subaqueous Volcanism*, Am. Geophys. Union Monogr., Washington D.C. 143–166.
- Fagel, N., 2007. Clay minerals, deep circulation, and climate. In: Hillaire–Marcel, C., de Vernal, A. (Eds.), *Paleoceanography of the Late Cenozoic, Methods*, 1, Elsevier, Amsterdam, 139–184.
- Fisher, R.V., Schmincke, H.-U., 1984. *Pyroclastic rocks*. Springer, Berlin Heidelberg, New York. pp 472.
- Fouquet, Y. et al. 1998. Extensive volcanoclastic deposits at the Mid–Atlantic Ridge axis; results of deep–water basaltic explosive volcanic activity? *Terra Nova* 10, 280–286.
- Glass, B.P., Koeberl, C., 2006. Australasian microtektites and associated impact ejecta in the South China Sea and the middle Pleistocene supereruption of Toba. *Meteor. Planet. Sci.*, 41, 305–326.
- Gupta, S.M., 1988. Radiolarian zonation and volcanic ash layers in two Quaternary sediment cores from the Central Indian Ocean Basin. *J. Palaeontol. Soc. India.*, 33, 59–71.
- Haflidason, H., Eriksson, J., Kreveld, S.V., 2000. The tephrochronology of Iceland and the North Atlantic region during the Middle and Late Quaternary: a review. *J. Quat. Sci.*, 15, 3–22.
- Head, J.W.I., Wilson, L., 2003. Deep submarine pyroclastic eruptions: theory and predicted landforms and deposits. *J. Volcanol. Geotherm. Res.*, 121, 155–193.
- Helo, C., Clague, D.A., Stix, J., 2008. Pyroclastic eruptions from Axial caldera, Juan de Fuca Ridge, NE Pacific Ocean. *IOP Conf. Ser. Earth Environ. Sci.*, 3:012005. doi:10.1088/1755-1307/3/1/012005.
- Helo, C., Longpre, M.-A., Shimizu, N., Clague, D.A., Stix, J., 2011. CO₂ rich magmas from Axial Seamount – A link to explosive eruptions on mid–ocean ridges? *Nature Geoscience* doi:10.1038/NGEO1104.

- Helo, C., Clague, D.A., Dingwell, D.B., Stix, J., 2013. High and highly variable cooling rates during pyroclastic eruptions on Axial Seamount, Juan de Fuca Ridge. *J. Volcanol. Geotherm. Res.*, 253, 54–64. doi: 10.1016/j.jvolgeores.2012.12.004.
- Horn, D.R., Delach, M.N., Horn, B.M., 1969. Distribution of volcanic ash layers and turbidites in the North Pacific. *Geol. Soc. Am. Bull.*, 81, 1715–1724.
- Iyer, S.D., 1999. Alteration of basaltic glasses from the Central Indian Ocean. *J. Geol. Soc. India.*, 54, 609–620.
- Iyer, S.D., Karisiddaiah., 1988. Morphology and petrography of pumice from the Central Indian Ocean Basin. *Indian J. Mar. Sci.*, 17, 333–334.
- Iyer, S.D., Gupta, S.M., Charan, S.N., Mills, O.P., 1999. Volcanogenic hydrothermal iron-rich materials from the southern part of the Central Indian Ocean Basin. *Mar. Geol.*, 158, 15–25.
- Iyer, S.D., Mascarenhas-Pereira, M.B.L., Nath, B.N. 2007. Native aluminium (spherules and particles) in the central Indian Basin sediments: Implications on the occurrence of hydrothermal events. *Mar. Geol.*, 240, 177–184.
- Iyer, S.D., Shyam Prasad, M., Gupta, S.M., Charan, S.N., 1997. Evidence for recent hydrothermal activity in the Central Indian Basin. *Deep-Sea Res.*, 44, 1167–1184.
- Iyer, S.D., Sudhakar, M., 1993. Coexistence of pumice and manganese nodule fields: evidence for submarine silicic volcanism in the Central Indian Basin. *Deep-Sea Res.*, 40, 1123–1129.
- Kalangukar, N.G., Iyer, S.D., Ilangovan, D., 2011. Physical properties, morphology and petrological characteristics of pumices from the Central Indian Ocean Basin. *Acta Geol. Sin.*, 85, 826–839.
- Kamesh Raju, K.A., 1993. Magnetic lineation, fracture zones and seamounts in the Central Indian Ocean Basin. *Mar. Geol.*, 109, 195–201.
- Krishna, K.S., Ramana, M.V., Rao, D.G., Murthy, K.S.R., Rao, M.M.M., Subrahmanyam, V., Sarma, K.V.L.N.S., 1998. Periodic deformation of oceanic crust in the central Indian Ocean. *J. Geophys. Res. (B: Solid Earth)*: 103, 17859–17875.
- Krishnaswami, S., Sarin, M.M., 1976. Atlantic surface particulates: composition, settling rates and dissolution in the deep sea. *Earth Planet. Sci. Lett.*, 32, 430–440.
- Le Bas, M.J., Le Maitre, R.W., Streckeisen, A., Zanettin, B., 1986. A chemical classification of volcanic rocks based on the total alkali silica diagram. *J. Petrol.*, 27, 745–750.
- Lee, M.Y., Chen, C.-H., Wei, K.-Y., Iizuka, Y., Carey, S., 2004. First Toba supereruption revival. *Geol.*, 32, 61–64.
- Lim, C., Ikehara, K., Toyoda, K., 2008. Cryptotephra detection using high-resolution trace-element analysis of Holocene marine sediments, southwest Japan. *Geochim. Cosmochim. Acta.*, 72, 5022–5036.
- Lowe, J.J., Turney, C.S.M., 1997. Vedde ash layer discovered in a small lake basin on the Scottish mainland. *J. Geol. Soc.*, 154, 605–612.
- McLennan, S.M., 2001. Relationship between the trace element composition of sedimentary rocks and upper continental crust. *Geochem. Geophys. Geosyst.* 2, doi: 10.1029/2000GC000109.

Maicher, D., White, J.D.L., 2001. The formation of deep-sea Limu o Pele. *Bull. Volcanol.*, 63, 482–496.

Martin-Barajas, A., Lallieri-Verges, E., 1993. Ash layers and pumice in the central Indian Basin: relationship from the formation of manganese nodules. *Mar. Geol.*, 115, 307–329.

Mascarenhas, M.B.L., 2015. Geochemical aspects of early diagenesis, submarine volcanism and hydrothermalism in an intraplate tectonic setting. Ph.D Thesis, Goa University, 269 pp.

Mascarenhas-Pereira, M.B.L., Nath, B.N., Borole, D.V., Gupta, S.M., 2006. Nature, source and composition of volcanic ash in sediments from a fracture zone trace of Rodriguez Triple Junction in the Central Indian Basin. *Mar. Geol.*, 229, 79–90.

Mascarenhas-Pereira, M.B.L., Nath, B.N., 2010. Selective leaching studies of sediments from a seamount flank in the Central Indian Basin: Resolving hydrothermal, volcanogenic and terrigenous sources using major, trace and rare-earth elements. *Mar. Chem.*, 121, 49–66.

Matthews, N.E., Smith, V.C., Costa, A., Durant, A.J., Pyle, D.M., Pearce, N.J.G., 2012. Ultra-distal tephra deposits from super-eruptions: Examples from Toba, Indonesia and Taupo Volcanic Zone, New Zealand. *Quart. Internatl.*, 258, 54–79.

Mudholkar, A., Fujii, T., 1995. Fresh pumice from the central Indian Basin: a Krakatau 1883 signature. *Mar. Geol.*, 125, 143–151.

Mukherjee, A.D., Iyer, S.D., 1999. Synthesis of the morphotectonics and volcanics of the Central Indian Ocean Basin. *Cur. Sci.*, 76, 296–304.

Mühe, R., Bohrmann, H., Garbe-Schönberg, D., Kassens, H., 1997. E-MORB glasses from the Gakkel Ridge (Arctic Ocean) at 87°N: evidence for the Earth's most northerly volcanic activity. *Earth Planet. Sci. Lett.*, 152, 1–9.

Nath, B.N., 2001. Geochemistry of sediments. In: SenGupta, R., Desa, E., (Eds.), *The Indian Ocean: A perspective*. Oxford & IBH; New Delhi (India) 2, 645–689.

Nath, B.N., Rao, V.P.C., Becker, K.P., 1989. Geochemical evidence of terrigenous influence in deep-sea sediments up to 8°S in the Central Indian Basin. *Mar. Geol.*, 87, 301–313.

Nath, B.N., Roelandts, I., Sudhakar, M., Plueger, W.L., 1992. Rare earth element patterns of the Central Indian Basin sediments related to their lithology. *Geophys. Res. Letts.*, 19, 1197–1200.

Nath, B.N., Sijinkumar, A.V., Borole, D.V., Gupta, S.M., Mergulhao, L.P., Mascarenhas-Pereira, M.B.L., Ramaswamy, V., Guptha, M.V.S., Possnert, G., Aldahan, A., Khadge, N.H., Sharma, R., 2013. Record of carbonate preservation and the Mid-Brunhes climatic shift from a seamount top with low sedimentation rates in the Central Indian Basin. *Boreas* 42(3), 762–778.

Pattan, J.N., Shane, P., Banakar, V.K., 1999. New occurrence of youngest Toba Tuff in abyssal sediments of the Central Indian Basin. *Mar. Geol.*, 155, 243–248.

Pattan, J.N., Shyam Prasad, M., Babu, E.V.S.S.K., 2010. Correlation of the oldest Toba Tuff to sediments in the central Indian Ocean Basin. *J. Earth Syst. Sci.*, 119, 531–539.

Peters, J.L., Murray, R.W., Sparks, J.W., Coleman, D. S., 2000. Terrigenous matter and dispersed ash in sediment from the Caribbean Sea; results from Leg 165. *Proceedings of the Ocean Drilling Program, Scientific Results, Leg 165*, pp. 115–124.

- Pimm, A.C., 1974. Sedimentology and history of the Northeastern Indian Ocean from Late Cretaceous to Recent. In: Initial Reports of the Deep Sea Drilling Project, Vol 22, (Eds) von der Borch, C.C., Sclater, J.G., et al., US Government Printing Office, Washington, 119–191.
- Plank, T., Ludden, J.N., Escutia, C., et al., 2000. Proceedings of the Ocean Drilling Program, initial reports, Izu–Mariana Margin; Proceedings of the Ocean Drilling Program, Part A, Initial Reports, 185.
- Pollard, A.M., Blockley, S.P.E., Lane, C.S., 2006. The chemical correlation of microtephras: numerical analysis of geochemical data. *Appl. Geochem.*, 21, 1692–1714.
- Pontbriand, C.W., Soule, S.A., Sohn, R.A., Humphris, S.E., Kunz, C., Singh, H., Nakamura, K., Jakobsson, M., Shank, T., 2012. Effusive and explosive volcanism on the ultraslow-spreading Gakkel Ridge, 85°E. *Geochem. Geophys. Geosys.*, 13, 1–22. doi: 10.1029/2012.GC004187.
- Rao, V.P., Nath, B.N., 1988. Nature, distribution and origin of clay minerals in grain size fractions of sediments from the manganese nodule field, Central Indian Ocean Basin. *Ind. J. Mar. Sci.*, 17, 202–207.
- Rose, W.I., Chesner, C.A., 1987. Dispersal of ash in the great Toba eruption, 75,000 years B. P. *Geology* 15, 913–917.
- Rickwood, P.C., 1989. Boundary lines within petrologic diagrams which use oxides of major and minor elements. *Lithos* 22, 247–263.
- Schipper, C.I., White, J.D.L., 2010. No depth limit to hydrovolcanic Limu o Pele: analysis of limu from Loihi Seamount. *Hawaii. Bull. Volcanol.*, 72, 149–164.
- Schulz, H., von Rad, U., Erienkeuser, H., 1998. Correlation between Arabian Sea and Greenland climate oscillations of the past 110,000 years. *Nature* 393, 54–57.
- Scudder, R.P., Murray, R., Plank, T., 2009. Dispersed ash in deeply buried sediment from the northwest Pacific Ocean: An example from the Izu–Bonin arc (ODP Site 1149). *Earth Planet. Sci. Lett.*, 284, 639–648.
- Scudder, R.P., Murray, R.W., Schindlbeck, J.C., Kutterolf, S., Hauff, F., Underwood, M.B., Gwizd, S., Lauzon, R., McKinley, C.C., 2016. Geochemical approaches to the quantification of dispersed volcanic ash in marine sediment. *Progress Earth Planet. Sci.*, 10.1186/s40645-015-0077-
- Shane, P., Westgate, J., Williams, M., Korisettar, R., 1995. New geochemical evidence for the youngest Toba Tuff in India. *Quat. Res.*, 44, 200–204.
- Smith, V.C., Pearce, N.J.G., Matthews, N.E., Westgate, J.A., Petraglia, M.D., Haslam, M., Lane, C.S., Korisettar, R., Pal, J.N., 2011. Geochemical fingerprinting of the widespread Toba tephra using biotite compositions. *Quat. Int.*, 246, 97–104.
- Sohn, R.A., Willis, C., Humphris, S., et al., 2008. Explosive volcanism on the ultraslow–spreading Gakkel ridge, Arctic Ocean. *Nature* 453, doi:10.1038/nature07075.
- Stranne, C., Sohn, R.A., Liljebladh, B., Nakamura, K., 2010. Analysis and modeling of hydrothermal plume data acquired from the 85°E segment of the Gakkel Ridge. *J. Geophys. Res.*, 115, C06028, doi:10.1029/2009JC005776.

- Straub, S.M., 1997. Multiple sources of Quaternary tephra layers in the Mariana Trough. *J. Volcanol. Geotherm. Res.*, 76, 251–276.
- Straub, S.M., Layne, G.D., 2003. The systematics of chlorine, fluorine and water in Izu arc front volcanic rocks. Implications for volatile recycling in subduction zones. *Geochim. Cosmochim. Acta.*, 67, 4179–4203.
- Sukumaran, N.P., Banerjee, R., Borole, D.V., Gupta, S.M., 1999. Some aspects of volcanic ash layers in the Central Indian Basin. *Geo-Mar. Lett.*, 18, 203–298.
- Taylor, R.N., Nesbitt, R.W., 1998. Isotopic characteristics of subduction fluids in an intra-oceanic setting, Izu–Bonin Arc, Japan. *Earth Planet. Sci. Lett.*, 164, 79–98.
- Taylor, S.R., McLennan, S.M., 1985. *The Continental Crust: Its Composition and Evolution*, Blackwell, Malden, Mass, 312 pp.
- Turney, C.S.M., Lowe, J.J., Davies, S.M., Hall, V.A., Lowe, D.J., Wastegård, S., Hoek, W.Z., Alloway, B., SCOTAV and INTIMATE groups. 2004. Tephrochronology of last termination sequences in Europe: a protocol for improved analytical precision and robust correlation procedures (a joint SCOTAV–INTIMATE proposal). *J. Quat. Sci.*, 19, 111–120.
- Urbat, M., Pletsch, T., 2003. Pleistocene deep-sea sediment in ODP Hole 1149A, Nadezhda Basin; sources, alteration, and age controls (0–800 ka). *Proc. Ocean Drill. Program, Sci. Results* 185, 21.
- Westgate, J., Shane, P.A.R., Pearce, N.J.G., Perkins, W.T., Korisettar, R., Chesner, C., Williams, M.A.J., Acharyya, S.K., 1998. All Toba tephra occurrences across peninsular India belong to the 75,000 yr BP eruption. *Quat. Res.*, 50, 107–112.
- White, J.D.L., Smellie, J.L., Clague, D.A., 2003. *Explosive Subaqueous Volcanism* (Eds.), White, J.D.L., Smellie, J. L., Clague, D.A. Am. Geophy. Union, Washington D.C., 1–24.
- Wohletz, K.H., 1983. Mechanisms of hydrovolcanic pyroclast formation: Size, shape, and experimental studies. *J. Volcanol. Geotherm. Res.*, 17, 31–63.
- Wulf, S., Kraml, M., Brauer, A., Keller, J., Negendank, J.F.W. 2004. Tephrochronology of the 100 ka lacustrine sediment record of Lago Grande di Monticchio (southern Italy). *Quat. Internatl.*, 122, 7–30.
- Ziegler, C.L., Murray, R.W., Hovan, S.A., Rea, D.K., 2007. Resolving eolian, volcanogenic, and authigenic components in pelagic sediment from the Pacific Ocean. *Earth Planet. Sci. Lett.*, 254, 416–432.

List of tables

Table 1: Details of sub-samples recovered from three sediment cores from the CIB.

Table 2: Abundance of glass shards (no of shards g^{-1}), age (ka), elemental concentration of Al (%), Sc (ppm), Cr (ppm), Nb (ppm) and Cr/Sc ratios (estimated in bulk sediments).

Table 3: Compositional (EDS) analysis (wt %) of glass shards for each layer obtained for each sub-samples from the three sediment cores. The data of core BC 8 are provided for comparison.

Table 4: Comprehensive facts of the several parameters studied of the volcanic horizons from the CIB sediment cores.

Figure captions

Figure 1: Major physiographic features of the Indian Ocean along with the location of the cores studied. Dashed lines indicate the fracture zones (Kamesh Raju et al., 1993).

Figure 2: Histograms of particle size distribution of the three volcanic horizons in the three cores studied using Laser particle size analyser.

Figure 3: Correlation of abundance of glass shards (no of shards g^{-1} of sediment) in BC 14, 20 and 25 with respect to age (ka) of the cores, with Cr/Sc ratio of bulk sediments and ash wt% based on Cr (●) and Nb (●) concentration normative calculations. Note the presence of volcanic activity indicated by abundance of glass shards, Cr/Sc ratio and single element normative calculations and excellent correlation in all the ash layers in all the three cores. Elemental concentration in ppm.

Figure 4: Electron micrographs of the investigated volcanic shards. The left hand panel shows the glass shards recovered from a shallow stratigraphic depth in the core corresponding to (70-75 ka) while the right hand panel shows the photographs of glass shards from deeper stratigraphic depths in the core. The glass morphologies recovered from the shallow depth (YTT) are dominant in bubble-wall shards while massive and blocky shards are dominant in the other horizons in all the cores studied. (a) Massive shards with sharp edges; (b) bubble wall shards with smooth and slightly curved surfaces; (c) angular, moderately vesicular shards with tubules extending the length of the shard; and (d) platy shard with angular and sharp edges.

Figure 5: $^{230}Th_{excess}$ profile in cores BC 14, BC 20 and BC 25 showing sedimentation rates of 0.27, 0.23 and 0.23 $cm\ ka^{-1}$, respectively.

Figure 6: (a) $Na_2O + K_2O$ vs. SiO_2 plot (TAS diagram). Nomenclature fields after Le Bas et al., (1986), with abbreviations: Tr, trachytic; T, tephrite; PhT, phonotephrite; TPh, tephri-phonolite; Ph, phonolite. A comparison of chemical composition of SRH from the study area with shards belonging to Toba volcanic. The shards of the five SRH from the study area plot in the rhyolitic field including glass reported to be of YTT and OTT age. Elemental data on shards from AAS 61/BC 14 were taken from 18-20 cm (~75 ka) (n=7) and 22-24 cm (85.5ka) (n=8), AAS 61/BC 20 were taken from 16-18 cm (74.5 ka) (n=5), 24-26 cm (109.2 ka) (n=6) and 32-34cm (146.3 ka) (n=10) and AAS 61/BC 25 were taken from 16-18 cm (73 ka) (n=6), 24-26 cm (107.3 ka) (n=10) and 32-34 cm (141.6 ka) (n=6).

(b) K_2O vs. SiO_2 plot of the shards, which shows all glasses with high SiO_2 plot in the high K series. Series boundaries after Rickwood (1989).

Figure 7: SiO_2 and K_2O (wt%) in the tephra from the SRH in the three cores versus age (ka). The elemental oxide compositions of tephra from the three cores at a given SRH are similar with marginal variation in composition.

Table 1

Core No	Latitude (°S)	Longitude (°E)	Sed. Rate (cm ka ⁻¹)	Water depth (m)	Length of core (cm)	Physical description	Sediment type
BC 8*	15 59.981	76 30.000	0.032	5010	20	0–8 cm: light brown, radiolarian ooze 8–20cm: black, indurated clays with volcanoclastic material	Red Clay
BC14	14 00.231	75 30.064	0.269	5145	36	0–10 cm: moderate brown 10–36 cm: light brown with intercalations	Siliceous ooze + Red Clay
BC 20	12 00.066	75 29.893	0.229	5200	40	0–10 cm: moderate brown 10–19 cm: light yellowish brown with greenish grey and moderate brown intercalations distinctly different from cores in the south	Siliceous ooze
BC25	10 59.964	75 29.927	0.233	5300	37	0–11 cm: Homogeneous moderate brown 11–17 cm: moderate brown to light yellowish brown >17 cm: light yellowish brown with grey layers at 22, 25, 32–37 cm.	Siliceous ooze

*Mascarenhas-Pereira et al., 2006

Table 2

Core No	BC 14							BC 20							BC 25							BC 8	
sed. rate	0.269							0.229							0.233							0.032	
Depth (cm)	abundance	Age	Alk	Sc	Cr	Nb	Cr/Sc	abundance	Age	Alk	Sc	Cr	Nb	Cr/Sc	abundance	Age	Alk	Sc	Cr	Nb	Cr/Sc	abundance	Age
0-2	NA	3.7	NA	NA	NA	NA	NA	73232	4.4	NA	NA	NA	NA	NA	10726	4.3	5.55	18	36	5.32	1.96		
2-4	21319	11.2	5.08	18.27	31.26	6.36	1.71	73972	13.1	5.4	NA	NA	NA	NA	21621	12.9	5.37	19	37	5.77	1.9		
4-6	23407	18.6	5.56	16.65	30.08	5.88	1.81	74566	21.8	5.17	10.59	34.39	5.80	1.76	26811	21.5	5.60	19	35	5.36	1.80		
6-8	27325	26.0	5.81	16.70	31.02	6.21	1.86	79338	30.6	5.00	17.59	34.68	5.49	1.97	83333	30.0	5.03	17	33	4.78	1.93		
8-10	36633	33.5	5.20	16.05	23.73	5.52	1.48	58385	39.3	4.65	16.85	35.87	5.55	2.13	145405	38.6	4.87	17	33	4.71	1.87		
10-12	46341	40.9	5.20	14.43	25.59	5.53	1.77	123333	48.0	4.53	16.11	33.97	5.58	2.11	141637	47.2	4.80	16	30	4.37	1.86		
12-14	56994	48.3	4.89	14.56	28.55	5.30	1.96	153500	56.8	4.74	16.34	31.91	5.35	1.95	130261	55.8	4.69	16	28	4.16	1.77		
14-16	85964	55.8	5.01	14.66	27.93	5.07	1.91	44078	65.5	5.00	15.85	30.54	5.36	1.93	208837	64.4	4.87	16	28	4.25	1.79		
16-18	89887	63.2	5.76	16.23	25.55	5.33	1.57	153846	74.2	4.97	15.55	34.51	5.60	2.22	498095	73.0	4.16	15	27	3.96	1.83		
18-20	110747	70.6	5.73	15.77	24.20	5.61	1.53	88108	83.0	5.16	15.74	31.81	5.79	2.02	125112	81.5	5.24	13	25	3.07	1.94		
20-22	88057	78.1	5.30	14.11	25.24	5.85	1.79	91596	91.7	5.21	14.14	26.05	6.75	1.84	99315	90.1	4.33	14	26	3.73	1.77		
22-24	129007	85.5	5.86	14.95	25.72	6.63	1.72	151875	100.4	5.02	14.11	25.37	5.90	1.8		98.7	5.56	15	25	3.94	1.65		
24-26	75268	92.0	6.43	16.93	25.21	6.45	1.49	206787	109.2	5.59	12.87	22.92	6.50	1.78	604000	107.3	6.06	14	24	4.01	1.68		
26-28								190513	117.9	5.45	12.99	17.78	6.59	1.37		115.9	6.16	15	24	4.03	1.68		
28-30								183505	126.6	5.59	13.02	22.30	6.72	1.71	451869	124.5	4.70	14	23	3.83	1.66		
30-32								135365	135.4	5.46	12.05	21.84	6.44	1.81		133.1	5.32	13	21	3.75	1.67		
32-34								683152	146.3	5.89	11.59	20.23	7.84	1.75	1017857	141.6	5.77	12	21	3.80	1.75		

abundant > 180
below 8cm

Table 3

Core No.	Depth (cm)	Grain	SiO ₂	Al ₂ O ₃	FeO*	MnO	MgO	CaO	TiO ₂	P ₂ O ₅	Na ₂ O	K ₂ O	Na ₂ O+ K ₂ O
BC 14	18–20	1	78.65	11.55	1.01	0.02	0.04	0.69	0.06	0.16	2.74	5.07	7.81
		2	78.88	11.3	1.03	0.06	0.1	0.8	0.19	nd	2.19	5.44	7.63
		3	78.31	11.67	1.01	0.12	0.17	0.77	0.12	nd	2.61	5.22	7.83
		4	78.4	11.84	0.81	0.01	0.03	0.59	0.16	nd	3.27	4.88	8.15
		5	78.83	11.42	0.76	0.04	0.22	0.55	0.16	nd	3	5.03	8.03
		6	78.78	11.8	0.9	0.03	nd	0.74	nd	nd	2.97	4.79	7.76
		7	78.24	11.87	0.86	nd	nd	0.85	0.13	nd	3.16	4.89	8.05
		average	78.58	11.64	0.91	0.05	0.11	0.71	0.14	0.16	2.85	5.05	7.89
	22–24	1	78.37	11.89	0.67	0.03	nd	0.74	nd	0.26	3.14	4.9	8.04
		2	78.45	11.7	0.86	0.03	nd	0.77	nd	0.14	2.96	5.09	8.05
		3	78.71	11.23	0.94	nd	0.08	0.81	0.16	nd	2.55	5.54	8.09
		4	78.59	11.9	0.76	nd	0.03	0.65	0.09	nd	2.77	5.21	7.98
		5	77.7	12.09	0.92	0.08	0.07	0.83	0.19	nd	3.2	4.92	8.12
		6	78.56	11.44	0.82	0.07	0.08	0.69	0.1	0.4	2.75	5.09	7.84
		7	78.79	11.49	0.86	0.15	0.06	0.7	nd	0.06	2.53	5.35	7.88
8		78.93	11.82	0.7	0.12	nd	0.53	nd	0.02	2.92	4.96	7.88	
average	78.51	11.70	0.82	0.08	0.06	0.72	0.14	0.18	2.85	5.13	7.99		

Continue..

Core No.	Depth (cm)	Grain	SiO ₂	Al ₂ O ₃	FeO*	MnO	MgO	CaO	TiO ₂	P ₂ O ₅	Na ₂ O	K ₂ O	Na ₂ O+ K ₂ O
BC 20	16-18	1	78.37	11.83	0.68	0.01	nd	0.7	0.07	nd	3.42	4.91	8.33
		2	78.61	11.69	0.69	nd	0.01	0.67	0.18	nd	3.08	5.07	8.15
		3	78.51	11.66	0.98	0.2	nd	0.77	0.05	nd	2.84	5	7.84
		4	78.68	11.55	0.74	0.1	0.1	0.75	0.15	nd	2.93	5	7.93
		5	78.73	11.17	1.01	nd	0.04	0.67	0.01	0.07	2.82	5.47	8.29
		avg	78.58	11.58	0.82	0.10	0.05	0.71	0.09	0.07	3.02	5.09	8.11
	24-26	1	76.26	10.46	2.06	0.38	nd	1.18	0.19	0.3	2.01	7.17	9.18
		2	78.64	11.56	0.67	0.16	0.14	0.52	nd	0.15	3.12	5.06	8.18
		3	78.76	11.76	0.78	0.05	nd	0.46	0.02	nd	3.51	4.66	8.17
		4	78.83	11.26	1.07	0.11	0.05	0.61	nd	nd	2.33	5.74	8.07
		5	78.71	11.29	1.06	0.11	0.04	0.8	0.03	nd	2.27	5.69	7.96
		6	78.77	11.87	0.79	nd	0.04	0.76	0.05	nd	2.69	5.02	7.71
	avg	78.33	11.37	1.07	0.16	0.05	0.72	0.07	0.23	2.66	5.56	8.21	
	32-34	1	78.73	11.28	0.89	0.03	0.08	0.86	nd	0.21	2.37	5.33	7.70
		2	78.79	11.09	0.93	0.06	0.06	0.79	0.02	0.1	2.33	5.62	7.95
		3	78.53	11.17	1.13	0.07	nd	1	0.25	0.07	2.33	5.32	7.65
4		78	10.38	1.53	0.13	nd	1.24	0.03	0.18	1.36	6.97	8.33	
5		78.89	11.11	1.01	0.05	0.06	0.94	0.03	0.04	1.75	5.98	7.73	
6		78.89	11.11	1.01	0.05	0.06	0.94	0.03	0.04	1.75	5.98	7.73	
7		78.68	10.01	1.33	0.09	0.02	0.88	0.03	0.15	1.48	7.11	8.59	
8		79.26	10.74	1.01	0.08	nd	0.74	nd	0.11	2.01	5.89	7.90	
9		79.09	10.86	1.02	0.03	nd	0.87	0.07	nd	1.92	6.05	7.97	
10		78.8	10.24	1.18	0.06	nd	0.75	0.15	0.05	1.36	7.16	8.52	
avg	78.77	10.80	1.10	0.07	0.04	0.90	0.08	0.11	1.87	6.14	8.01		

Continue..

Core No.	Depth (cm)	Grain	SiO ₂	Al ₂ O ₃	FeO*	MnO	MgO	CaO	TiO ₂	P ₂ O ₅	Na ₂ O	K ₂ O	Na ₂ O+ K ₂ O
BC 25	16–18	1	78.86	11.37	0.93	0.17	nd	0.59	nd	nd	2.98	5.12	8.10
		2	77.39	11.9	1.37	0.12	0.13	0.73	0.12	0.33	2.72	5.2	7.92
		3	78.55	11.78	0.75	0.05	0.05	0.66	0.11	nd	3.1	4.96	8.06
		4	79.35	10.47	1.4	0.2	0.04	0.67	0.16	nd	1.71	6	7.71
		5	79.07	11.19	1.02	0.05	0.1	0.78	0.02	nd	2.06	5.71	7.77
		6	78.23	11.23	1.17	nd	nd	0.74	0.21	0.16	2.32	5.95	8.27
		avg	78.58	11.32	1.11	0.12	0.08	0.70	0.12	0.25	2.48	5.49	7.97
	24–26	1	79.05	10.14	1.05	0.15	0.04	0.71	0.03	0.16	1.44	7.03	8.47
		2	79.12	10.73	0.97	0.03	0.04	0.82	0.06	0.08	1.7	6.24	7.94
		3	77.86	10.88	1.5	0.05	0.1	0.98	0.24	0.05	1.67	6.66	8.33
		4	79.14	10.86	0.87	0.07	0.08	0.73	0.02	0.21	1.91	5.9	7.81
		5	77.86	9.81	1.65	0.14	0.05	1.11	0.33	nd	1.18	7.66	8.84
		6	79.32	10.77	0.9	0.06	nd	0.77	nd	0.03	1.71	6.22	7.93
		7	78.73	10.69	1.07	0.06	0.06	0.95	0.09	0.13	1.63	6.42	8.05
		8	78.94	10.43	1.07	0.04	0.06	1.05	0.14	nd	1.49	6.6	8.09
		9	77.09	9.94	1.85	0.14	0.04	1.32	0.21	nd	1.45	8	9.45
		10	78.93	10.63	1.12	0.06	0.02	0.92	nd	0.1	1.44	6.65	8.09
	avg	78.60	10.49	1.21	0.08	0.05	0.94	0.14	0.08	1.56	6.74	8.30	
	32–34	1	78.76	11.75	0.75	0.12	nd	0.78	nd	nd	2.81	5.02	7.83
2		77.94	12.19	0.96	nd	0.1	0.55	0.04	nd	3.41	4.8	8.21	
3		78.08	11.68	1.03	0.11	0.16	0.83	0.24	nd	2.98	5.31	8.29	
4		77.98	11.86	0.97	0.15	nd	0.65	0.12	nd	3.2	5.06	8.26	
5		78.38	11.57	1.13	nd	0.04	0.77	0.27	0.11	2.36	5.37	7.73	
6		78.08	12.04	0.66	0.09	nd	0.71	0.07	0.1	3.56	4.69	8.25	
avg		78.20	11.85	0.92	0.12	0.10	0.72	0.15	nd	3.05	5.04	8.10	
Core No	Depth (cm)	Sample	SiO ₂	Al ₂ O ₃	FeO*	MnO	MgO	CaO	TiO ₂	P ₂ O ₅	Na ₂ O	K ₂ O	Na ₂ O+K ₂ O
BC 8	8–20	26	75.3	12.3	0.9	nd	nd	0.64	0.07	nd	4.45	4.47	8.92
		29	75.4	12.7	0.65	nd	nd	0.55	0.09	nd	5.55	3.9	9.45
		23	76	12	0.93	nd	nd	0.68	0.07	nd	3.86	4.76	8.62
		2	76.3	12.2	0.91	nd	nd	0.66	0.05	nd	3.37	4.61	7.98
		3	75.3	12.5	0.7	nd	nd	0.57	nd	nd	4.76	4.33	9.09
		4	76.3	11.8	0.8	nd	nd	0.6	0.1	nd	3.7	4.7	8.4
		Grain 1	74.7	11.8	0.85	0.07	nd	0.53	0.1	nd	5.75	4.46	10.21
		Grain 2	73.9	12.4	0.72	0.09	nd	0.62	0.04	nd	6.35	4.17	10.52
		Grain 4	75.6	11.2	1.26	nd	nd	0.78	0.13	nd	2.36	6	8.36
		Grain 5	74.8	12.1	0.9	0.05	nd	0.74	0.07	nd	5.01	4.52	9.53
		Grain 6a	75.1	11.6	0.89	0.08	nd	0.64	0.05	nd	4.63	5.01	9.64
		Grain 6b	74.8	12	0.81	0.07	nd	0.55	0.07	nd	5.57	4.6	10.17
		Grain 7	75	11.1	1.2	0.1	nd	0.8	nd	nd	3.6	5.6	9.2
		Grain 8	74.3	12.3	0.7	0.07	nd	0.62	0.12	nd	6.13	4.38	10.51
average	75.3	11.9	0.91	0.07	nd	0.65	0.08	nd	4.41	4.79	9.21		

Table 4

Cryptotephra (ka)	Shard rich horizon (ka)	Core No	BC 14	BC 20	BC 25	Description of shards
34		Depth (cm)	8-10			bubble wall and massive types
	70-75		18-20	16-18	16-18	dominated with bubble wall types
	85		22-24			dominated with massive and blocky types with minor amount of bubble wall and platy types
	107-109			24-26	24-26	
	141-146			32-34	32-34	

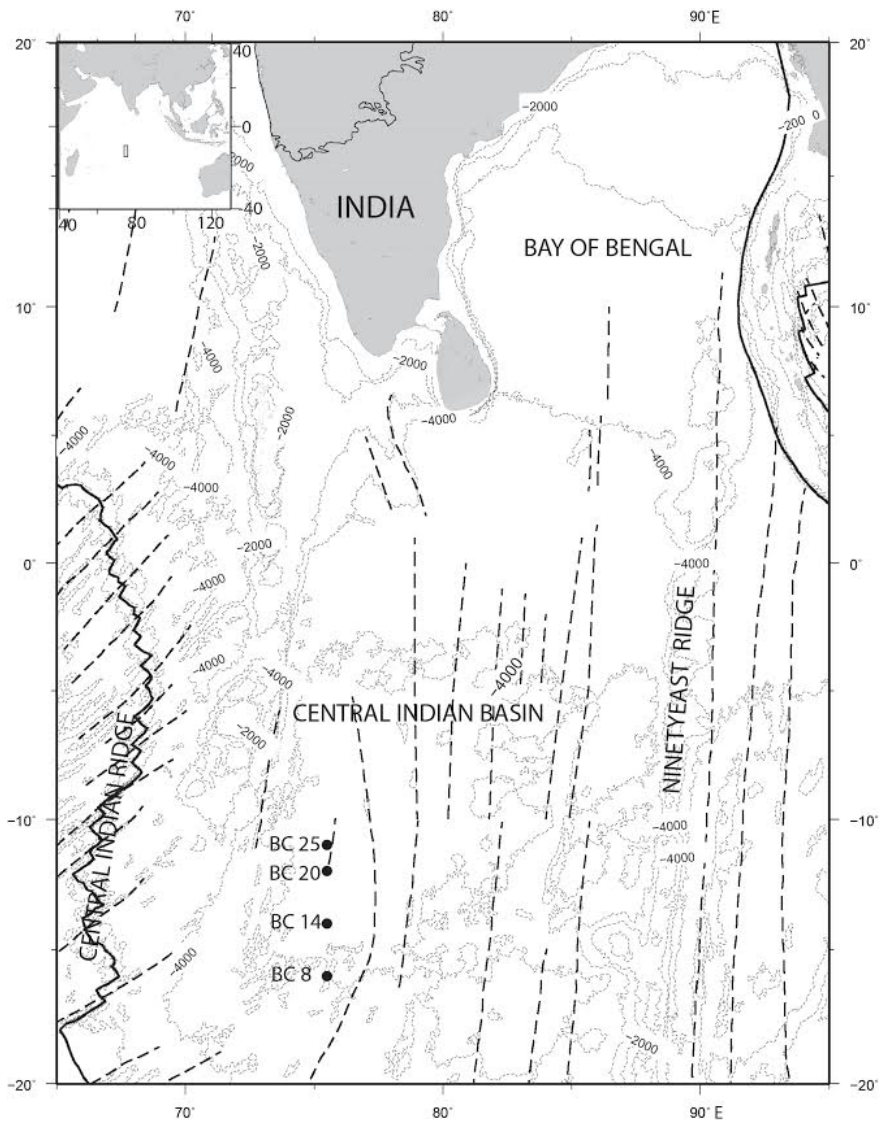


Figure 1

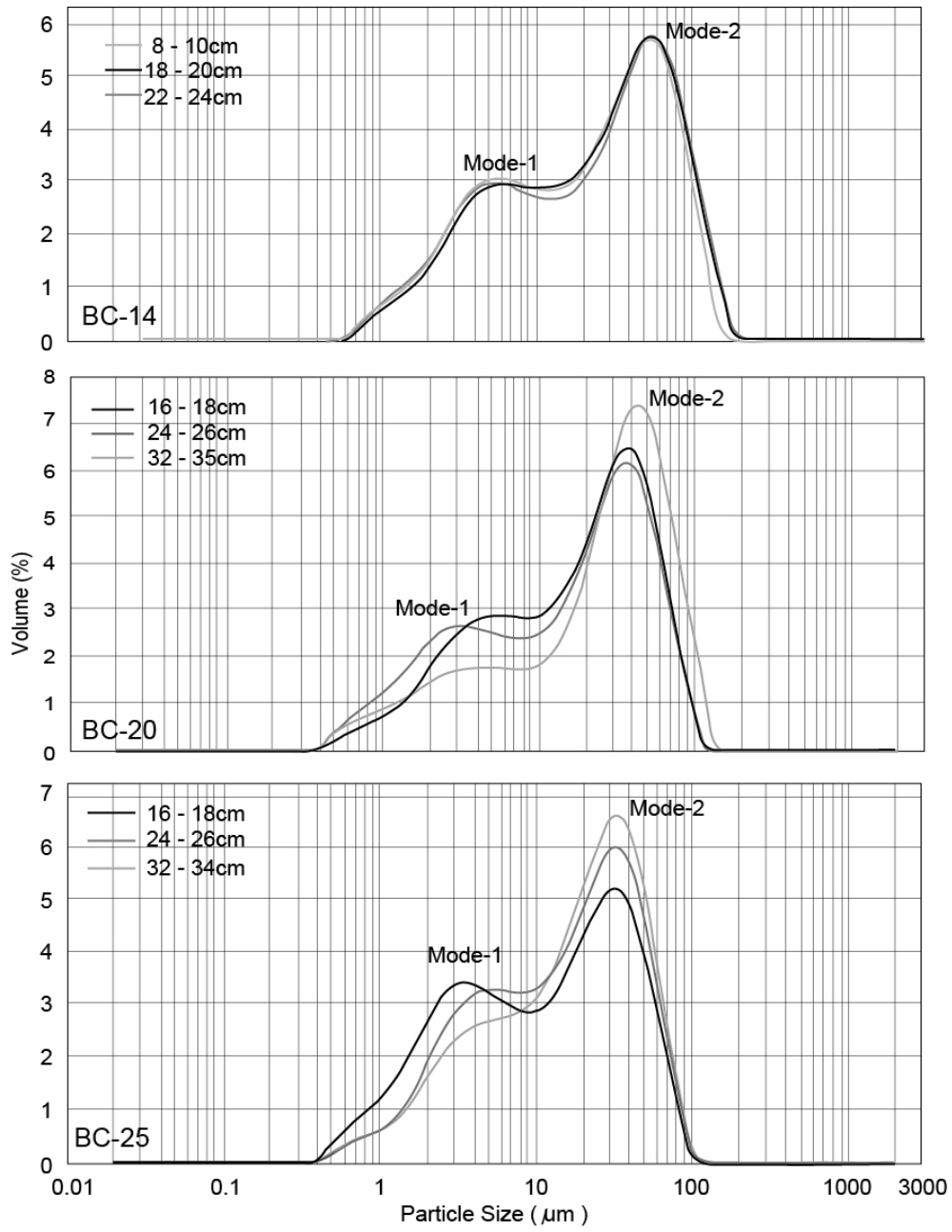


Figure 2

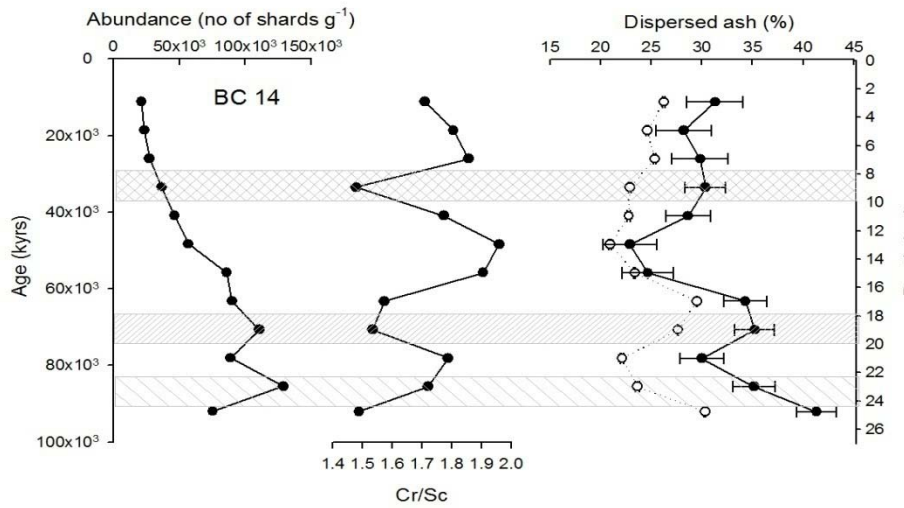
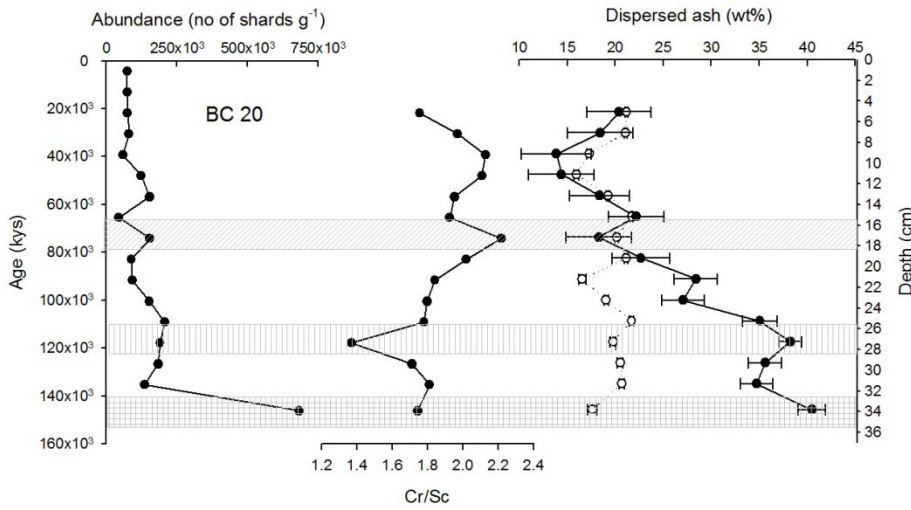
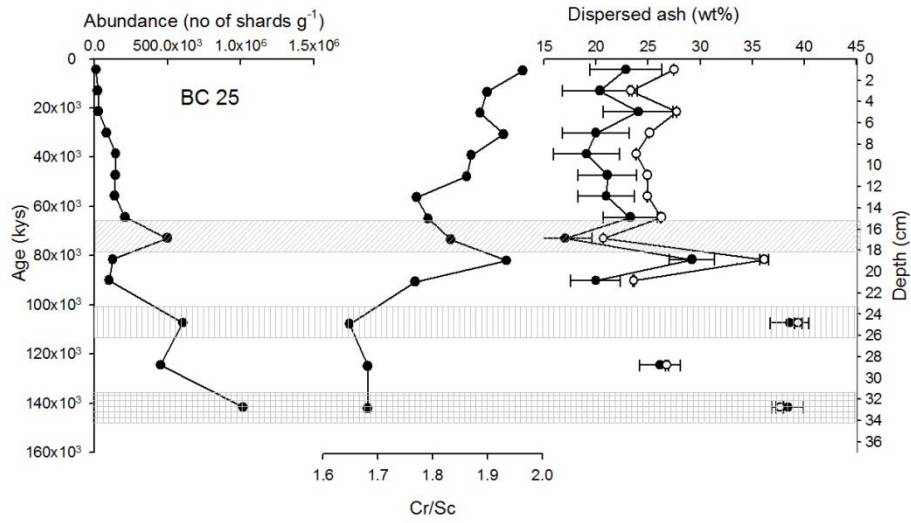


Figure 3

A AAS 61, BC 20, 16–18 cm

24–26 cm

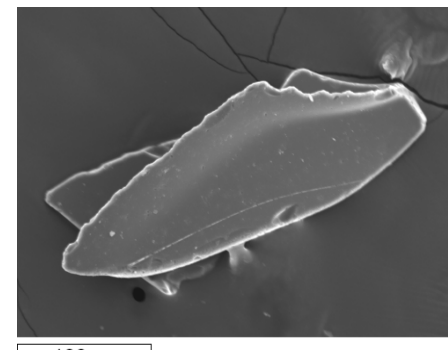
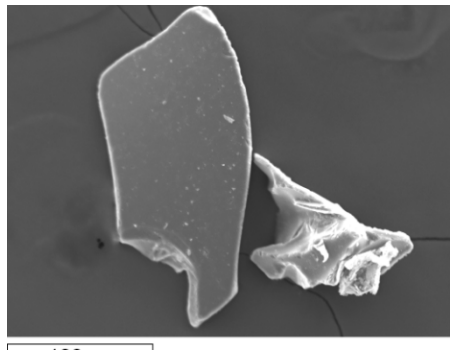
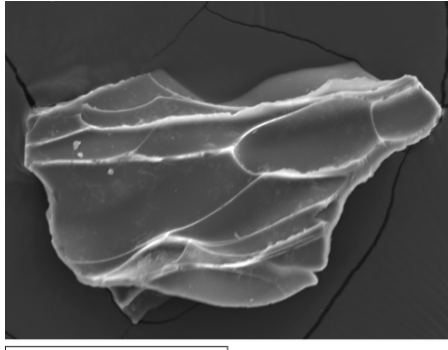
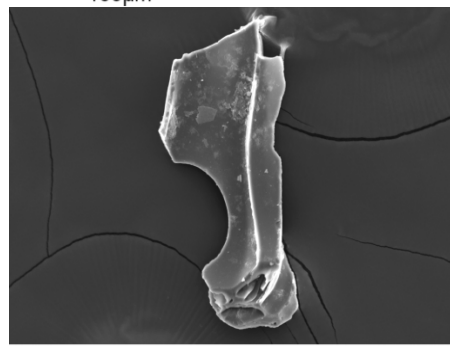
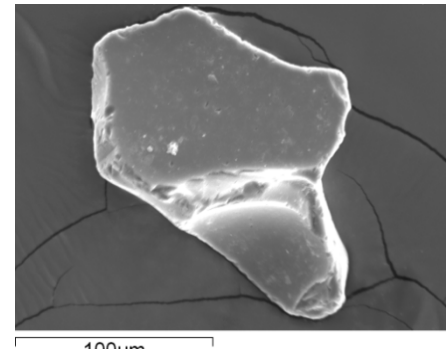
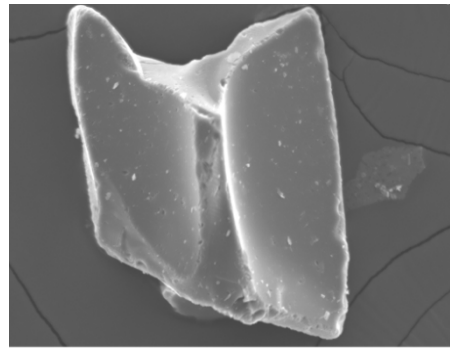
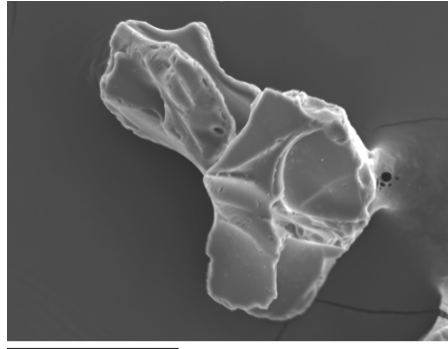
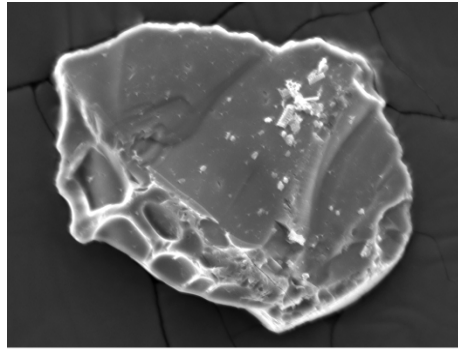


Figure. 4 A

B AAS 61, BC 25, 16–18 cm

32–34 cm

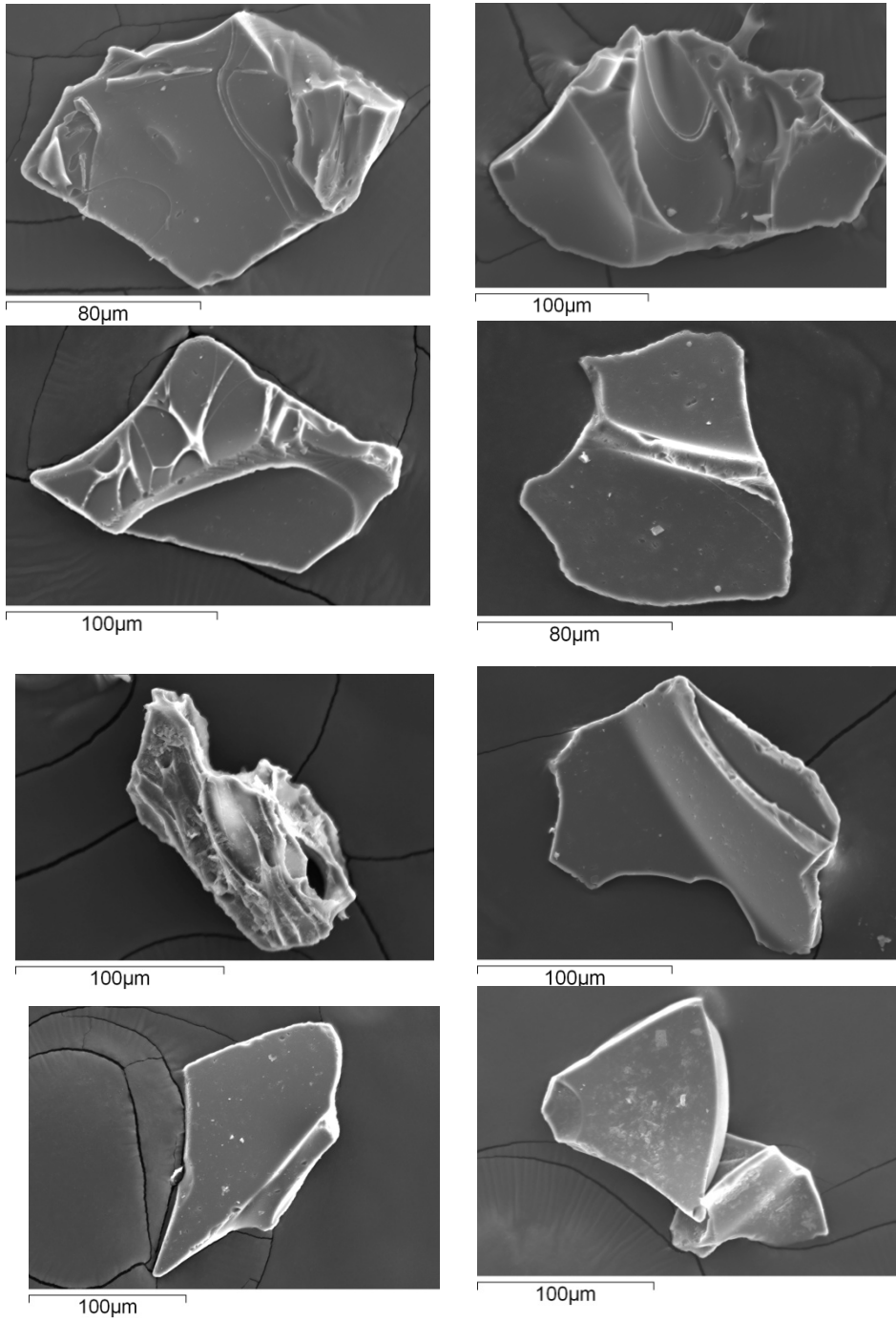


Figure 4 B

C AAS 61, BC 14, 18–20 cm

22–24 cm

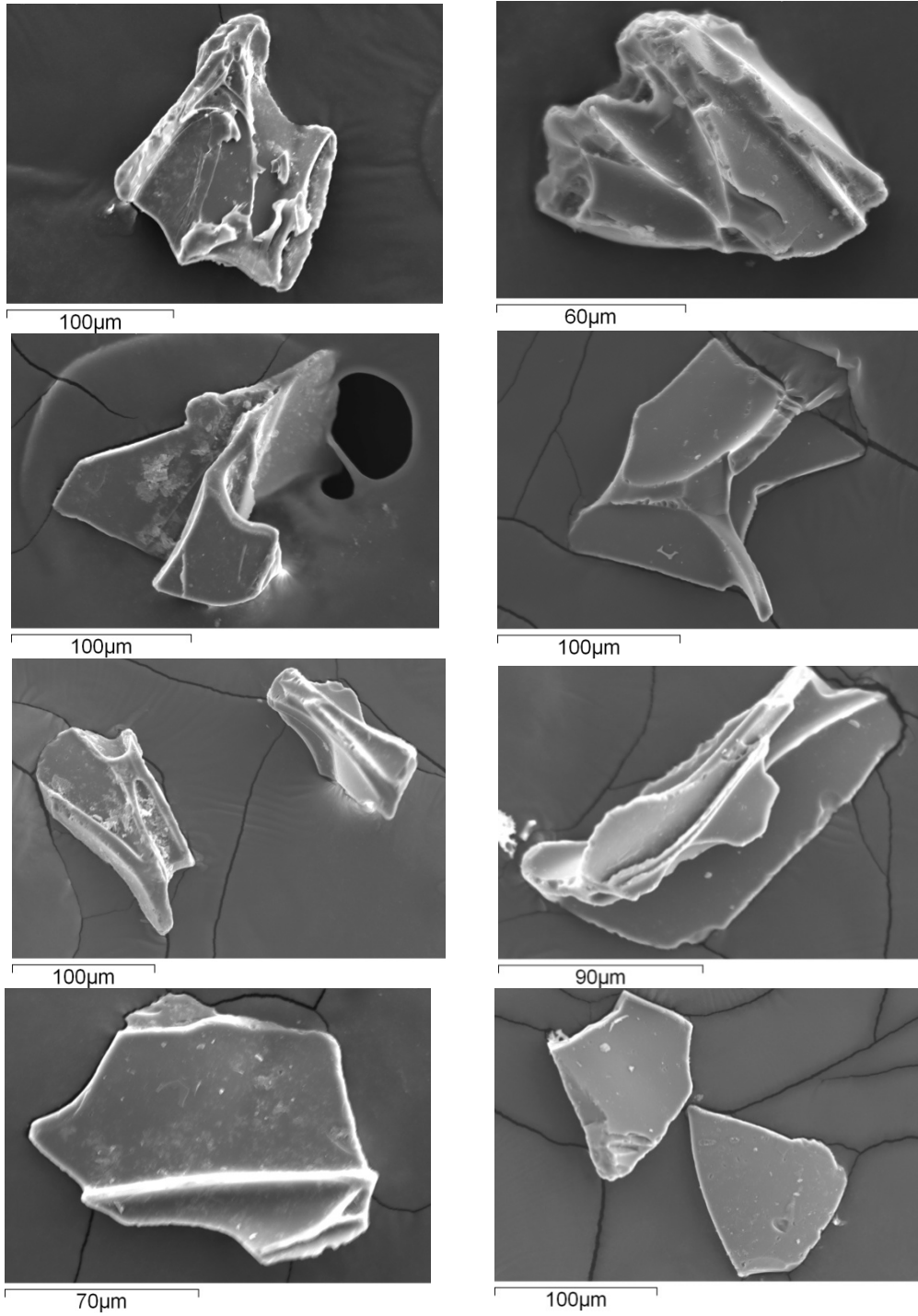


Figure 4 C

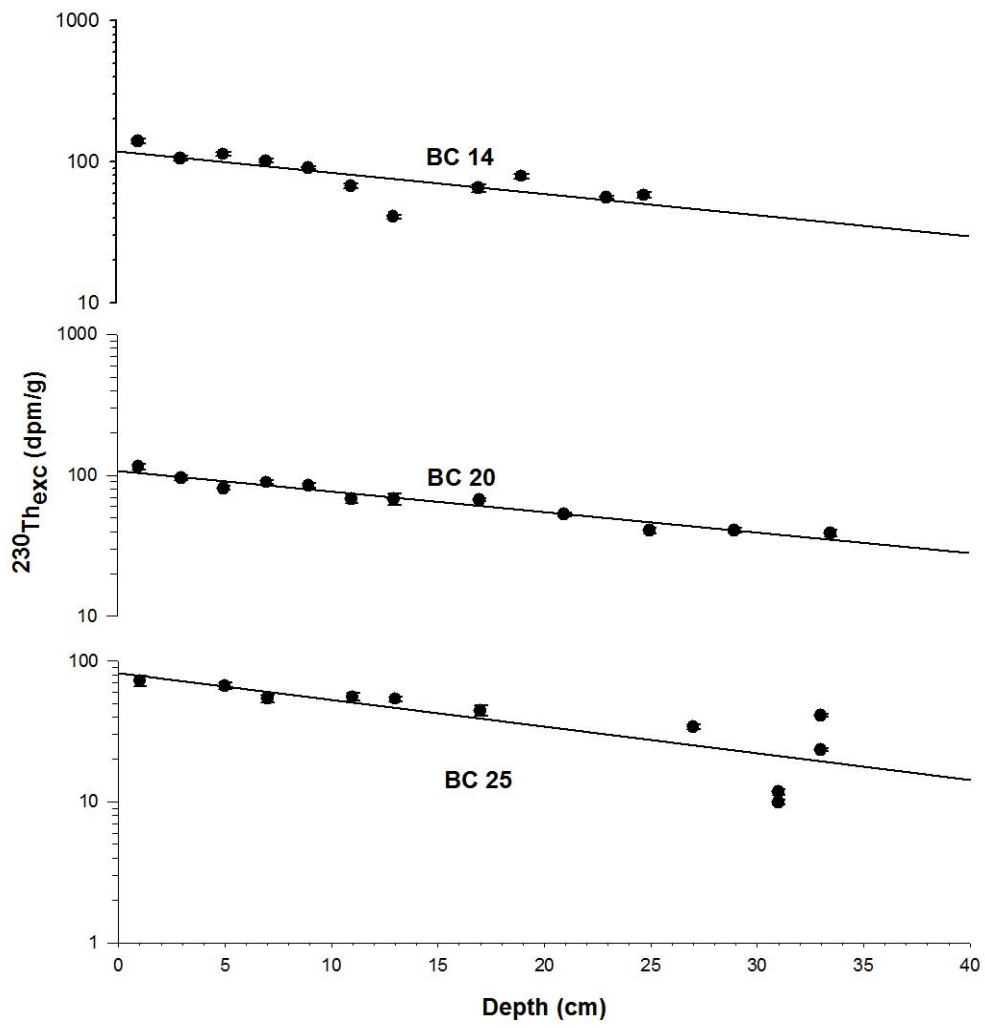
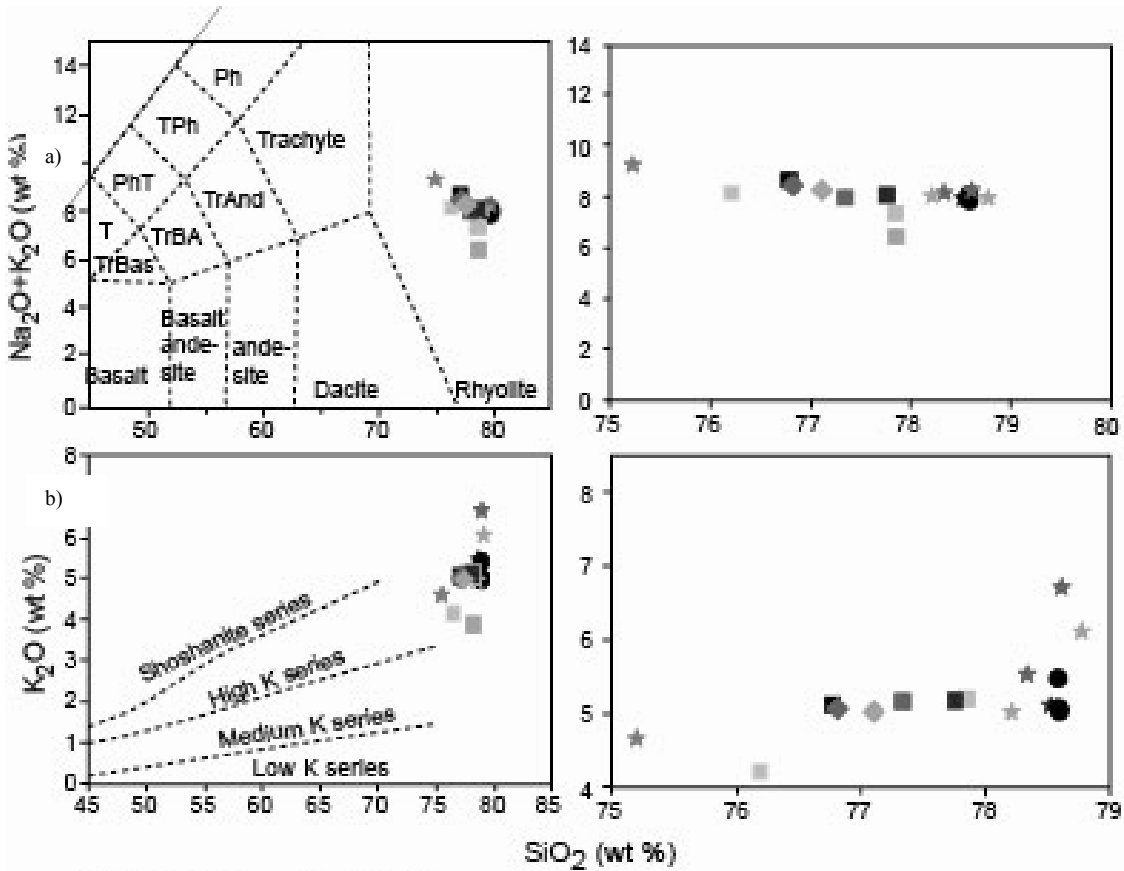


Figure 5



Study area Literature

- | | |
|----------------|--|
| | OTT |
| (●) 70 - 75ka | (■) average of 42 glass shards from different locations (Glass and Koeberl, 2006), |
| (★) ~ 85ka | (■) average of shards from 17°S, (■) 13°S, (■) CIB (Pattan et al., 2010) |
| (★) 107-109ka | (■) Layer D and (■) Layer E from ODP 758 (Dehn et al., 1991) |
| (★) 142-146 ka | YTT |
| (★) >180ka | (◆) 8 cores from siliceous oozes in CIB (3° to 14°S) (Pattan et al., 1999) |
| | (◆) distal fallout sites in India and Malaysia (Shane et al., 1995) |

Figure 6

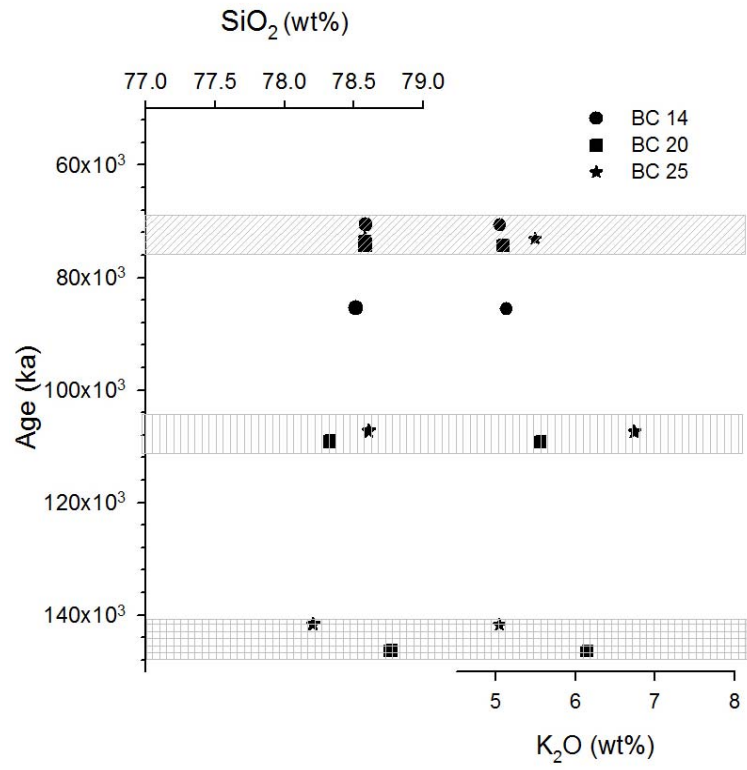


Figure 7